Journal of Medicinal Chemistry

Article

Purine-type Compounds Induce Microtubule Fragmentation and Lung Cancer Cell Death through Interaction with Katanin

Ting-Chun Kuo, Ling-Wei Li, Szu-Hua Pan, Jim-Min Fang, Jyung-Hurng Liu, Ting-Jen R. Cheng, Chia-Jen Wang, Pei-Fang Hung, Hsuan-Yu Chen, Tse-Ming Hong, Yuan-Ling Hsu, Chi-Huey Wong, and Pan-Chyr Yang

J. Med. Chem., **Just Accepted Manuscript** • DOI: 10.1021/acs.jmedchem.6b00797 • Publication Date (Web): 18 Aug 2016

ACS Publications

Journal of Medicinal Chemistry is published by the American Chemical Society. 1155 Sixteenth Street N.W., Washington, DC 20036

Purine-type Compounds Induce Microtubule Fragmentation and Lung Cancer Cell Death through Interaction with Katanin

Ting-Chun Kuo[¶], *Ling-Wei Li*[¥], *Szu-Hua Pan*[*, ¶, #, £], *Jim-Min Fang*[*, ¥], *Jyung-Hurng Liu*[¢, §, |, ǂ], *Ting-Jen Cheng*[η], *Chia-Jen Wang*[&, ζ], *Pei-Fang Hung*[&], *Hsuan-Yu Chen*[ʒ], *Tse-Ming Hong*[ø], *Yuan-Ling Hsu*[#], *Chi-Huey Wong*[η, δ], *and Pan-Chyr Yang*[|, φ, Θ, δ].

¶ Ph.D. Program in Translational Medicine, National Taiwan University and Academia Sinica, Taipei, Taiwan

¥ Department of Chemistry, National Taiwan University, Taipei 106, Taiwan.

Graduate Institute of Medical Genomics and Proteomics, College of Medicine, National Taiwan University, Taipei 100, Taiwan

£ Genome and Systems Biology Degree Program, National Taiwan University and Academia Sinica, Taipei 106, Taiwan

¢ Department of Life Sciences, National Chung Hsing University, Taichung 402, Taiwan

§ Institute of Genomics and Bioinformatics, National Chung Hsing University, Taichung 402, Taiwan

| Agricultural Biotechnology Center, National Chung Hsing University, Taichung 402, Taiwan

ǂ Rong Hsing Research Center for Translational Medicine, National Chung Hsing University 402, Taichung, Taiwan.

η Genomics Research Center, Academia Sinica, Taipei 115, Taiwan.

& Department of Internal Medicine, National Taiwan University College of Medicine, Taipei 100, Taiwan

ζ Institute of Stem Cell and Translational Cancer Research, Chang Gung Memorial Hospital at

ʒ Institute of Statistical Science, Academia Sinica, Taipei 115, Taiwan

Ø Institute of Clinical Medicine, National Cheng Kung University College of Medicine, Tainan 701, Taiwan.

φ Institute of Biomedical Sciences, Academia Sinica, Taipei 115, Taiwan

Θ NTU Center for Genomic Medicine, National Taiwan University, Taipei 100, Taiwan.

∆ Senior authors.

* Corresponding authors.

KEYWORDS

Non-small-cell lung cancer; Microtubule targeting agent; Microtubule fragmentation; Katanin.

ABSTRACT

Microtubule targeting agents (MTAs) constitute a class of drugs for cancer treatment. Despite many MTAs have been proven to significantly improve the treatment outcomes of various malignancies, resistance has usually occurred. By selection from a 2-million entry chemical library based on the efficacy and safety, we identified purine-type compounds that were active against lung small cell lung cancer (NSCLC). The purine compound **5a** (GRC0321) was an MTA with good effects against NSCLC. Lung cancer cells H1975 treated with **5a** could induce microtubule fragmentation, leading to G2/M cell cycle arrest and intrinsic apoptosis. Compound **5a** directly targeted katanin and regulated the severing activity of katanin, which cut the cellular microtubules into short pieces and activated c-Jun N-terminal kinases (JNK). The microtubule fragmenting effect of **5a** is a unique mechanism in MTAs. It might overcome the resistance problems that most of the MTAs have faced.

INTRODUCTION

Lung cancer remains the leading cause of cancer-related mortality worldwide[1]. Although treatment advances have been made over the past 20 years, the response rate and prognosis of lung cancer patients remain poor[2, 3], and drug resistance has become one of the main causes of treatment failure[4]. Therefore, the development of anti-cancer drugs with novel mechanisms for lung cancer treatment is urgently needed.

Microtubules, long, hollow cylinders composed of polymerized α- and β-tubulin dimers, are an important component of the cytoskeleton. They play an irreplaceable role in a variety of cellular functions, including the maintenance of cell shape, polarity, vesicles and mitosis[5].

During mitosis, microtubules form the mitotic spindle, which separates the daughter chromosomes to the opposite ends of the poles. Because of this characteristic, microtubules become a suitable target for anti-cancer agents to kill rapidly dividing cancer cells[5-7]. Usually, the tubular polymers of tubulin can grow as long as 50 μm, and the processes of microtubule assembly and disassembly are highly dynamic and are controlled by GTP binding and hydrolysis events. Regulating this unstable characteristic of microtubules is crucial for cells to respond to different circumstances[8, 9]. Until now, many microtubule-targeting agents (MTAs) have been found to target this property of the microtubules, and they can be further classified into two groups: stabilizing and destabilizing agents. The microtubule-stabilizing agents, including taxanes and epothilones, can stabilize the polymer formation of microtubules and increase the polymer mass of the microtubules in the cells. In contrast, microtubule-destabilizing agents, such as the vinca alkaloids, depolymerize microtubules and decrease the polymer mass. To date, taxanes and a series of vinca alkaloids are two major MTAs that are used in current chemotherapeutic regimes with excellent effects on different human malignancies[5, 10]. However, after a prolonged treatment, the clinical activity of the MTAs will usually be reduced due to drug resistance[11, 12]. As a result, there is an ongoing effort to develop novel agents within each class, to improve their efficacy and overcome drug resistance.

In addition of developing novel MTAs, targeting microtubule-associated proteins (MAPs) is identified as an alternative mechanism to overcome the drug resistance problem of MTAs[13]. The MAPs are a class of proteins that associate with microtubules, usually at the ends of the filaments. They regulate the dynamic behaviors of the microtubules by enhancing the rate of microtubule growth or increasing the frequency of catastrophes of microtubules[13]. Among MAPs, stathmin and tau are two important target proteins for cancer therapy. Inhibiting the expression

of stathmin by anti-stathmin ribozyme, either as monotherapy or in combination with chemotherapeutic agents, has been demonstrated to reduce cell proliferation and increase apoptosis in breast cancer cells[14]. The expression level of tau protein is associated with the sensitivity of paclitaxel in breast cancer cells, thus decreasing tau expression would make breast cancer cells hypersensitive to paclitaxel[15]. In addition, a class of proteins known as microtubule severing proteins can also bind to microtubules and regulate their dynamics by cutting microtubules into short fragments[16]. For example, katanin, one of the microtubule severing proteins, is a heterodimer hydrolase that is composed of two subunits called p60 and p80, according to their molecular weights. The p60 subunit is the catalytic subunit that contains the AAA (ATPase associated with diverse cellular activities) region, which functions in microtubule severing activity. The other subunit, p80, serves a regulatory function[17, 18]. Although katanin has received little attention in the context of cancer in the past, some of the literature has recently revealed its potential roles in cancer formation and progression. Ye and colleagues found that the expression of katanin p60 was up-regulated in prostatic adenocarcinomas[19]. Sudo and Maru also found that LAPSER1, a tumor suppressor gene in prostate cancer, participated in cytokinesis by interacting with katanin p80, and the disruption of this interaction might cause genetic instability and cancer[20].

Recently, our laboratory has been devoted to screening novel effective inhibitors to overcome drug resistance in non-small-cell lung cancer (NSCLC). In this study, GRC0321 (compound **5a**) was one of the compounds that was selected from a 2-million compound library through a two-step high-throughput screening of several lung cancer cell lines with different epidermal growth factor receptor (EGFR) status (including EGFR wild type and EGFR mutants)[21]. The purine-type compound **5a** was selected due to its excellent *in vitro* and *in vivo*

activities against NSCLC. We demonstrated that **5a** could disrupt the microtubule into small fragments in NSCLC cells by interacting with microtubule severing proteins katanin p60 and p80. The damage further activated c-Jun N-terminal kinases (JNK)-related signaling pathways, which caused G2/M cell cycle arrest and triggered mitochondria-mediated intrinsic apoptosis. Our results demonstrated that microtubule severing proteins could serve as a target for anti-cancer therapy.

RESULTS

Identification of purine-type compounds that possess NSCLC inhibitory activities. Through high-throughput screening of efficient drugs for the treatment of NSCLC cells, we found a purine-type compound **5a**, which was active to several lung cancer cell lines with IC_{50} values of 0.23–0.33 μM (Table 1). The cytotoxic effect of **5a** in NSCLC cells is less related to EGFR status in these cells.

Table 1. Inhibitory activities of **5a** against different lung cell lines.

Cell line[a]	IC_{50} (μM)	Cell line[a]	IC_{50} (μM)
H1975	0.24 ± 0.03	CL1-0	0.24 ± 0.01
PC9	0.33 ± 0.01	CL1-5	0.28 ± 0.01
PC9/gef	0.25 ± 0.01	A549	0.23 ± 0.02
NBE	21.7 ± 1.6		

[a] CL1-0, CL1-5 and A549 are human lung adenocarcinoma cell lines with wide-type EGFR. PC9 is a human lung adenocarcinoma cell line with EGFR exon-19 deletion. H1975 and PC9/gef are two human lung adenocarcinoma cell lines with different resistant mechanisms to EGFR TKIs. H1975 harbors EGFR T790M

mutation and PC9/gef acquires EGFR TKIs resistance by long-term and low-dose treatment of EGFR TKIs *in vitro*. NBE is a human normal bronchial epithelial cell.

To further investigate the structure–activity relationship, we synthesized a series of derivatives with varied aryl moieties at the C2 and N9 positions. Scheme 1 shows the synthetic route to the purine compounds **5a**–**g** by consecutive coupling reactions of diaminomaleonitrile (**1**) with isocyanates **2a**–**c** and aldehydes **4a**–**e**.[22] The phenyl isocyanates **2a**–**c** (1.05 equiv) that bear 2-methoxy, 3-CO_2Me or 4-CO_2Me substituents were added to diaminomaleonitrile to afford the corresponding urea compounds **3a**–**c**, which then underwent condensation reactions with substituted benzaldehydes **4a**–**e** (1.05–2.0 equiv) to yield the desired 8-oxopurine products **5a**–**g**, which have an amido group at C6 and two aryl substituents at the N9 and C2 positions.

Scheme 1. Synthesis of purine-type compounds **5a**–**5g**.

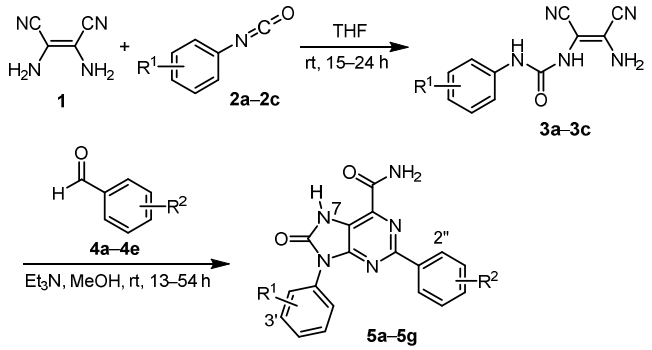

Phenyl isocyanate R^1 =	Benzaldehyde R^2 =	Purine product (Yield, %)[a]
2-OMe	4-OC_2H_5	**5a** (32)
2-OMe	4-OH	**5b** (20)
2-OMe	4-OC_4H_9	**5c** (20)
2-OMe	4-OC_6H_{13}	**5d** (30)
3-CO_2Me	4-OC_2H_5	**5e** (39)
4-CO_2Me	4-OC_2H_5	**5f** (52)
3-CO_2Me	4-Ph	**5g** (50)

[a] Total yield for two steps.

The growth inhibitory activity of **5a**–**5g** against H1975 was examined, and the IC_{50} values were determined by MTT assays (Table 2). The effect of the R^1 substituent in the N9-aryl group was variable. Compound **5e**, which has a CO_2Me substituent at the *meta*-position of the N9-aryl group, showed superior inhibitory activity (IC_{50} = 0.19 μM) compared with the hit **5a** (IC_{50} = 0.30 μM), whereas the analog **5f** has a *para*-CO_2Me substituent that exhibited lower activity (IC_{50} = 4.73 μM). In contrast, the effect of the R^2 substituent in the C2-aryl group was dramatic. Alternation of R^2 from ethoxy in **5a** to hydroxyl (**5b**), butoxy (**5c**), hexoxy (**5d**) or phenyl (**5g**) caused a large decrease in the inhibition.

Table 2. Inhibitory activities of purine-type compounds against the growth of H1975 lung cancer cells.

Compound	IC_{50} (μM)	Compound	IC_{50} (μM)
5a	0.30 ± 0.03	**5f**	4.73 ± 0.16
5b	5.80 ± 0.13	**5g**	> 20.0
5c	4.66 ± 0.05	**6e**	7.91 ± 0.18
5d	> 5.0	**8**	> 10.0
5e	0.19 ± 0.02	**9**	26.3 ± 0.3

Compound 5a inhibits lung cancer cell growth *in vitro* and *in vivo*. The purine-type compound **5a** was selected for further efficacy testing and to explore its action mechanism *in vitro* and *in vivo*. We first examined the cytotoxic activity of **5a** in different human NSCLC cells by MTT assay. As the results show in Figure 1A and Table 1, **5a** caused NSCLC cell death in a concentration-dependent manner, with the IC_{50} values in the range of 0.26 to 0.33 μM.

Compound **5a** was relatively non-toxic to the normal bronchial epithelial (NBE) cells, with an IC_{50} value of 21.66 μM. To further investigate the long-term effect, the colony formation assay was conducted to observe whether **5a** would interfere with the ability of single cells to form a growing colony. The results indicated that a 14-day treatment of **5a** inhibited the colony formation of the H1975 cells with an IC_{50} of 0.13 μM (Figure 1B). These data suggested that **5a** can inhibit NSCLC cell growth *in vitro*.

To explore the *in vivo* antitumor efficacy of **5a**, athymic nude mice that bear established subcutaneous H1975 tumors were treated intraperitoneal with **5a** twice a week at 2 mg/kg versus a vehicle control (n = 8 for each group). Figure 1C showed that **5a** at this dosage markedly reduced the H1975 tumor size to 930.4 ± 324.8 mm^3 ($P < 0.01$) compared with 1699.3 ± 413.3 mm^3 of the vehicle-treated group on day 28. The body weights of the test mice and the biochemical markers of the liver and kidney functions, including GOT, GPT, BUN and Cre, were not significantly affected after a 28-day treatment, which indicated that **5a** was well tolerated at the dosage of 2 mg/kg (Figure s1 in Supporting Information (SI)).

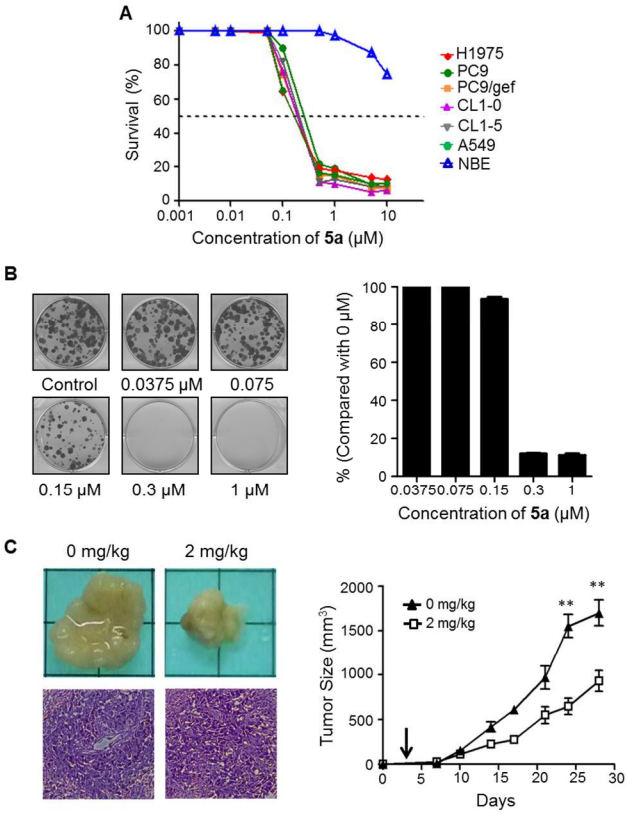

Figure 1. Compound 5a inhibits tumor growth in vitro and in vivo. (A) Inhibitory activities of **5a** against different human non-small-cell lung cancer cell lines. The cells were treated with **5a** for 72 h, and cell proliferation was examined by MTT assay. Data are expressed as the mean of four determinations. (B) H1975 cells were treated with **5a** (300 nM) for 14 days. The colonies were fixed and stained with crystal violet and counted. Data are expressed as the mean ±SEM of three determinations. (C) H1975 cells were injected subcutaneously into the right flank region of nude mice. Three days after the injection, the mice were treated with vehicle (DMSO) or **5a** (2 mg/kg) twice a week intraperitoneally for 28 days. Representative tumor images and H&E-stained sections of tumors taken from mice treated for 28 days with either vehicle or **5a** are shown. The tumor size was measured with a caliper rule every time before compound delivery. Data are presented as the mean tumor volumes of mice in both the treatment and vehicle groups on the days of pre-treatment.

Compound 5a induces cell cycle arrest and apoptosis in H1975 lung cancer cells. To confirm that the cytotoxic effect of **5a** was caused by an apoptotic cell death, the **5a**-treated H1975 lung cancer cells were co-stained with annexin V and propidium iodide (PI), and the positive staining population was analyzed by flow cytometry. The results indicated that positive annexin V- and PI-stained H1975 cells increased significantly after the treatment with **5a** (Figure 2A). This experiment suggested that the **5a**-treatment could cause apoptosis in H1975 cells. When further dissecting the potential apoptotic pathways that are activated by **5a**, the expression levels of several specific apoptotic markers were detected by immunoblotting. As expected, the cleaved form of two important regulatory proteins in the apoptotic pathway, caspase-3 and PARP-1, appeared after compound treatment. The appearance of cleaved caspase-9 implied that a mitochondria-mediated apoptotic pathway was being activated (Figure 2B). Therefore, the protein level of the Bcl-2 family proteins and the location of cytochrome C were also detected. The protein level of Bak and Bax, two pro-apoptotic proteins in the Bcl-2 family, did not change significantly after the treatment with **5a**. However, in the blotting results, we could see a band that had a molecular weight that was higher than that of the total form of Bcl-2 protein, which was detected after the compound treatment (star mark in Figure 2C). This band might be correlated to the phosphorylation form of the Bcl-2 protein, which increased after compound treatment. As is known, cytochrome C release from mitochondria to the cytosol is another marker that is frequently found after apoptotic induction. Here, we also attempted to clarify whether the compound treatment could cause cytochrome C release in the H1975 cells. The data showed that a 6-hour treatment of **5a** induced an increase in the cytosolic level of cytochrome C

(Figure 2D). All of these results indicated that **5a** could induce cell apoptosis in H1975 lung cancer cell lines.

In addition to the apoptotic inducing effect, we also explored whether the treatment of **5a** could have any effect on the H1975 cell cycle progression. We found that compound treatment also caused cell cycle arrest in H1975 lung cancer cells. The flow cytometric analysis of the cell cycle by PI staining showed that **5a** induced an increase in the cell population at the G2/ M phase (Figure 2E).

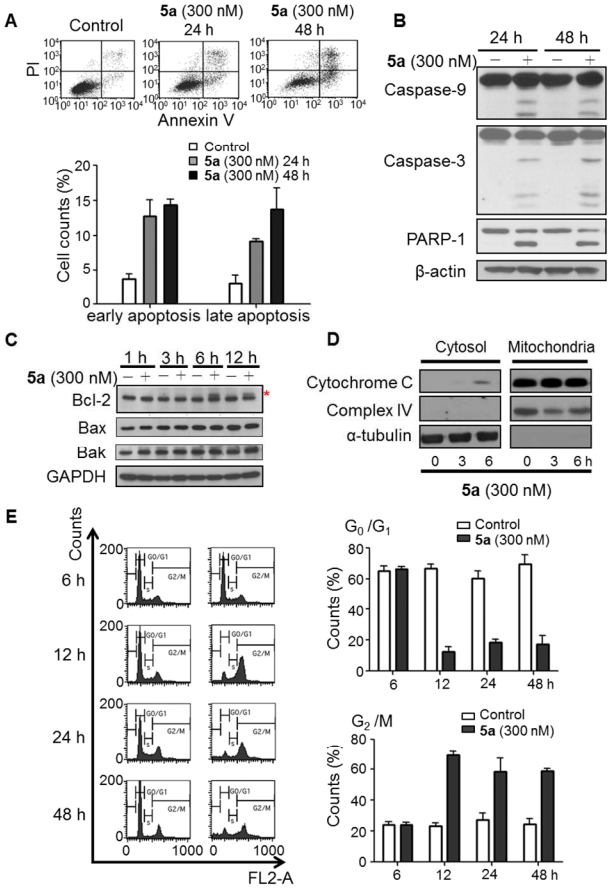

Figure 2. Compound 5a causes cell cycle arrest and induces cell apoptosis in H1975 lung cancer cells. H1975 cells were treated with 300-nM **5a** for the indicated time periods. Then, the cells were harvested for (A) annexin V-PI double staining of apoptosis FACScan flow cytometer. Data are expressed as the mean ±SEM of three determinations. (B and C) The protein

expressions were detected by immunoblotting. The data are representative of three independent experiments. (D) The cytosolic and mitochondrial fractions were obtained for the detection of the cytochrome C protein level by immunoblotting. (E) The cells were fixed and stained with PI to analyze the DNA content with a FACScan flow cytometer. The data are representative of three independent experiments.

Compound 5a activates the JNK-related signaling pathway and induces cell apoptosis. To characterize the molecular changes that were induced by **5a**, the human phospho-kinase antibody array was used. H1975 cells were harvested after a 9-hour treatment with 300 nM of **5a**, and the assay was then applied to the cell lysate. Cells treated with DMSO alone were used as controls. The results showed that treatment with **5a** increased the signal intensity of phosphorylated JNK (JNK pT183/Y185 and pT221/Y223) and phosphorylated c-Jun (c-Jun pS63) when compared with the results in the control group (Figure 3A). To further verify the results, cells treated with **5a** (300 nM) for 6 and 12hours were harvested, and the phosphorylation levels of these two proteins were detected by immunoblotting. The results showed that a dramatic up-regulation of phospho-JNK and phospho-c-Jun was observed after the compound treatment (Figure 3B).

To further determine the role of JNK-related signaling pathways in the mechanism of **5a**-induced cell apoptosis, a JNK inhibitor, 1,9-pyrazoloanthrone (SP600125), was adopted. As the results demonstrated, SP600125 could inhibit the activation of the JNK-related signaling pathways and reverse the apoptotic effects induced by **5a**. The cleaved form of caspase-3 and PARP-1 decreased after combining SP600125 with the compound (Figure 3C). Additionally, SP600125 also reduced the percentage of cells that had positive annexin V and PI staining after

treatment with **5a** (Figure 3D). Overall, these data suggested that JNK kinase and its related signaling pathways played important roles in the apoptotic cascade of **5a**.

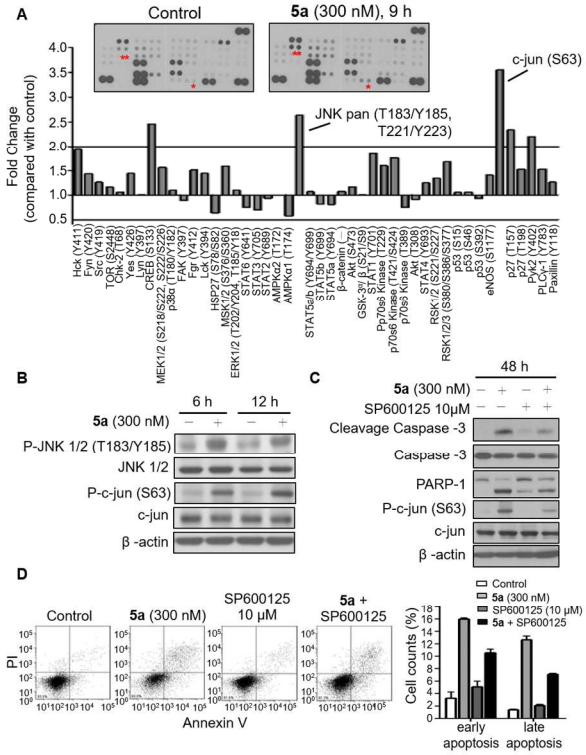

Figure 3. JNK-related signaling pathway involved in 5a-induced cancer cell apoptosis. (A) H1975 cells were incubated in the absence or presence of **5a** (300 nM) for 9 h. The cells were then harvested and lysed to detect the phosphorylation level of the proteins included in the human phosphor-kinase antibody array. The phosphorylation level of particulate proteins was quantified using the computerized image analysis system ImageJ. (B) H1975 cells treated with **5a** (300 nM) were harvested and lysed to detect the existence of phospho-JNK and phospho-c-Jun. The data are representative of three independent experiments. (C) H1975 cells were incubated in the indicated agent (**5a**, 300 nM; SP600125, 10 μM) for 48 h. Then, the cells were harvested and lysed to examine the expression levels of cleavage caspase-3, PARP-1 and phospho-c-Jun. The data are representative of three independent experiments. (D) H1975 cells

were treated with the indicated agent (**5a**, 300 nM; SP600125, 10 μM) for 48 h. Then, the cells were harvested for the annexin V-PI double staining of the apoptosis FACScan flow cytometer. The data are expressed as the mean ±SEM of three determinations.

Compound 5a induces fragmentation of microtubules and interrupts its organization in H1975 cells. The results showed that **5a**-treatment would cause cell cycle arrest at the G2/M phase and apoptosis in H1975 lung cancer cells, which led us to hypothesize that **5a**-treatment could also interfere with microtubule rearrangement due to its critical role in G2/M regulation. To test this idea, the organization of intracellular microtubules was first detected by immunofluorescence in H1975 cells. The in situ labeling of α-tubulin by antibodies demonstrated that **5a** would induce microtubule fragmentation (Figure 4A). An *in vitro* microtubule assembly assay was also performed to separate the assembled and disassembled microtubules into particulate and soluble fractions by centrifugation. The data showed that a 1-hour exposure of **5a** significantly reduced the amount of α-tubulin in the particulate fraction (the relative expression percentage of the soluble form vs. polymer form was 68% vs. 32% at 300 nM treatment and 75% vs. 25% at 600 nM; Figure 4B). The results from the *in vitro* microtubule assembly assay confirmed the microtubule-damaging effects of **5a** that were observed by the immunofluorescence staining. To further clarify the change in the microtubule structure after treatment with **5a**, a gel filtration chromatography method was applied to roughly determine the length of the microtubule in the H1975 cancer cells. The results showed that α-tubulin protein was detected in the latter fraction in the **5a**-treatment group compared to the DMSO control group. Moreover, there were fewer fractions that contained α-tubulin protein in the treatment

group compared to the control group (Figure 4C). These results indicated that **5a** reduced the length of the microtubule in H1975 lung cancer cells.

All of the above data indicated that **5a** interfered with the microtubule structure of H1975 lung cancer cells. Next, the turbidity assay for tubulin polymerization and depolymerization was adopted to examine whether **5a** displayed a direct regulatory function in microtubule assembly. As demonstrated in Figure 4D and 4E, in the presence of GTP at 37 °C, the tubulins were triggered to polymerize in a time-dependent manner. Nocodazole, vincristine and paclitaxel were used as reference agents to compare with **5a**. Surprisingly, according to the results, we found that **5a** did not influence the dynamics of microtubule polymerization and depolymerization (Figure 4D and 4E).

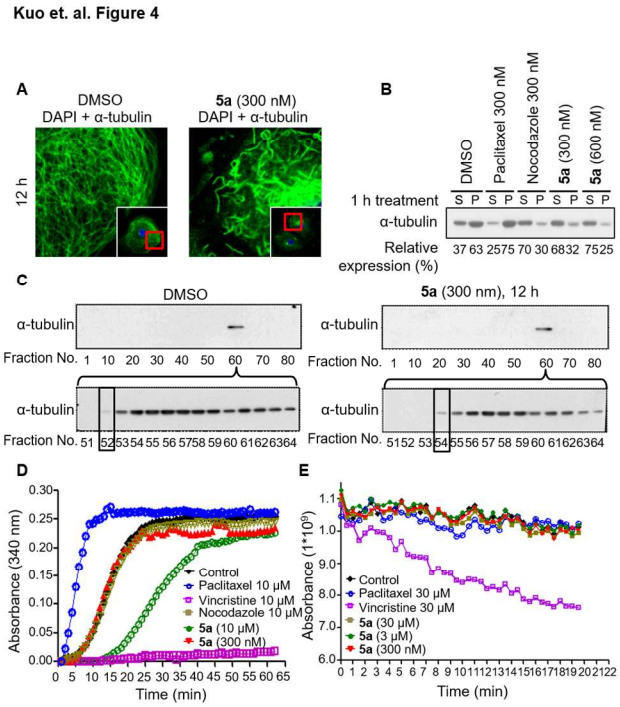

Figure 4. Treatment of 5a interrupts microtubule organization in H1975 lung cancer cells. (A) H1975 cells were incubated with vehicle or **5a** (300 nM) for the indicated times. Then, the cells were fixed and stained with anti-α-tubulin primary antibody. FITC-labelled secondary antibodies were used (green fluorescence), and the protein was detected by a confocal laser microscopic system. The nuclei were detected by DAPI staining (blue fluorescence). (B) H1975 cells were incubated with vehicle, **5a**, paclitaxel or nocodazole for 1 h. Then, the cells were harvested and separated into soluble (S, tubulin monomer) and particulate form (P, tubulin polymers), and the level of α-tubulin protein in each fraction was detected by immunoblotting. The protein level of α-tubulin was quantified using the computerized image analysis system ImageJ. (C) H1975 cells were incubated in the absence or presence of **5a** (300 nM) for 12 h. Then, the cells were harvested and lysed for gel filtration chromatography. The drop-by-drop flowthrough was collected in ~0.5-mL fractions. The protein level of α-tubulin in each fraction was detected by immunoblotting. (D) Purified tubulins were incubated at 37 ^{o}C with GTP in the vehicle (control) or in the presence of **5a** (10 μM or 300 nM), paclitaxel (10 μM), vincristine (10 μM) or nocodazole (10 μM). Tubulin polymerization was examined turbidimetrically. Data are expressed as the mean of three determinations. (E) Purified tubulins were incubated with GTP and paclitaxel at 37 ^{o}C for 30 min and then were held at room temperature for at least 1 h to obtain microtubule stock. The microtubule stock was further incubated at 37 ^{o}C with GTP in the vehicle (control) or in the presence of **5a** (10 μM, 3 μM or 300 nM), paclitaxel (30 μM) or vincristine (30 μM). Tubulin depolymerization was examined turbidimetrically. The data are expressed as the mean of three determinations.

Using a biotin-annexed probe to identify katanin as a direct target protein. To identify the target proteins of **5a**, its analogs carrying azido or diazirinyl group in the C2-aryl moiety were first designed as photoaffinity probes. Two analogs were synthesized by the coupling reactions of **3a** with 4-azidobenzaldehyde or 3-(4-(formylphenyl)-3-(trifluoromethyl)-3*H*-diazirine. However, the utilization of these two compounds as photoaffinity probes was hampered due to their instability, poor solubility and low inhibitory activity. Alternatively, we consider transforming the active compound **5e** (IC_{50} = 0.19 μM) into the desired probe using biotin as the reporter unit. As shown in Scheme 2, ester **5e** was subjected to saponification to give acid **6e**, which underwent the amide-forming reaction with amine **7** in the presence of *N*,*N*,*N*′,*N*′-tetramethyl-*O*-(1*H*-benzotriazol-1-yl)uronium hexafluorophosphate (HBTU, 1.0–1.2 equiv) and *N*,*N*-diisopropylethylamine (DIEA, 1.0–1.2 equiv), to afford the corresponding amide product **8**. The Boc protecting group in **8** was readily removed by treatment with trifluoroacetic acid (TFA) at room temperature, and the exposed amino group was successfully linked to D-(+)-biotin (1.0 equiv) via the amide bond-forming reactions, producing **9**.

The biotin-annexed **9** was used as a probe to catch the target proteins. After incubating with H1975 cell lysate, the proteins that were bound to **9** were pulled down by streptavidin-conjugated beads. Katanin p60 and p80 were visualized by immunoblotting (Figure 5A). As a control, the biotin linker that lacked the purine moiety could not trap katanin p60 or p80.

Scheme 2. Synthesis of amides **8** and the biotin-annexed probes **9**.

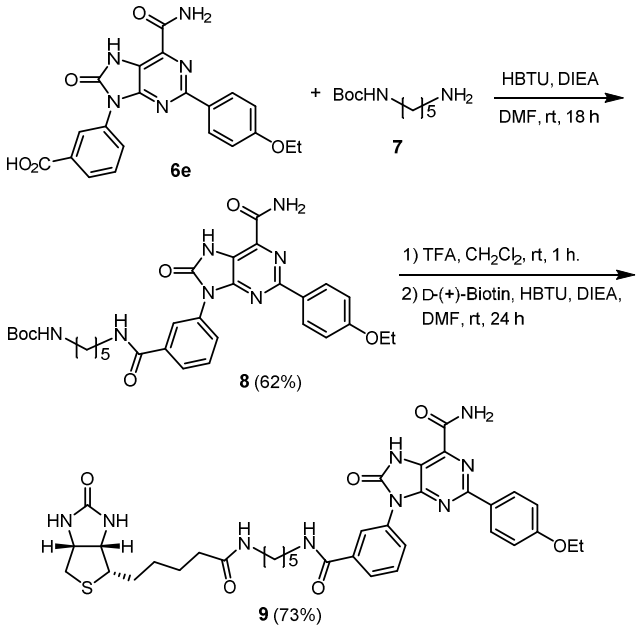

Molecular computation of pharmacophore models and p60–5a complex models. To correlate the chemical structures of the purine-type compounds to their NSCLC inhibition activities in a quantitative manner, we selected the compounds with certain IC_{50} values (Table 2) to generate the 3D-QSAR pharmacophore models. The results for the top ten pharmacophore hypotheses and their statistical parameters are shown in Table 3. In this study, the first pharmacophore hypothesis (Hypo-1) is the best because this model has the lowest total cost value (45.488), the largest cost difference (54.763), the lowest root-mean-square deviation (RMSD) value (0.699), and the highest correlation coefficient (0.984). Hypo-1 includes one hydrogen-bond acceptor (HBA), one hydrogen-bond donor (HBD), one hydrophobic feature (HY), and one ring aromatic feature (RA). The 3D spatial arrangement and distance constraints of these features are represented in Figure 5B. The features of Hypo-1 mapped onto **5a** are shown in Figure 5C. HBA is mapped onto the 8-oxo group, HBD is mapped onto the amino

moiety of the 6-carboxamide group, RA is mapped onto the C2-aryl group, and HY is mapped onto the tip of the ethoxy substituent in the C2-aryl group.

To demonstrate the predictive power of Hypo-1, regression analysis was used to estimate the activity of each training-set compound. As shown in Table 4, all of the training-set compounds showed an error value of less than 2. An error value below 10 indicated that only one order of magnitude of difference was observed in the discrepancy between the estimated and actual activity. The most active **5e** (IC_{50} = 0.19 μM) showed a fitness score value of 7.46 when mapped to Hypo-1, whereas the least active **6e** (IC_{50} = 7.91 μM) showed a fitness value of 6.04. This result indicates that Hypo-1 is a reliable model that consists of reasonable chemical features of the training-set compounds and accurately estimates the experimental activity of the training-set compounds. The calculated IC_{50} values through this 3D-QSAR pharmacophore model supports that **5a** and its analogue **5e** have the most potent inhibitory activity. Therefore, small molecules that completely satisfy the chemical feature arrangement of Hypo-1 could be good candidates for NSCLC inhibition. However, the high structural homology among the compounds used in this study combined with their small activity range made this 3D-QSAR pharmacophore model slightly imperfect. For example, the smaller difference (54.763) between the total and null cost values suggests that Hypo-1 might not have more than 90% statistical significance as a model. This difference value should be greater than or equal to 60, according to the Discovery Studio (DS) manual.

Although we found that katanin p60 and p80 can be pulled down by **9**, an analogue of **5a** (Figure 5A), we do not know whether **5a** binds to p60 or p80 or the interface between p60 and p80. Because **5a** shares a similar purine scaffold with ATP, we hypothesized that **5a** could bind to the catalytic AAA domain of p60. To assess this possibility, we modeled the homo-hexameric

p60 structure using the crystal structure of transitional endoplasmic reticulum ATPase p97 from mouse (PDB ID: 3CF1)[23] as the template. The sequence alignment indicated that human p60 shares 30% sequence identity with mouse p97, but the protein structure prediction server[24] Phyre2 suggested that the confidence score for this model is 100%. The docking software AutoDock Vina[25] successfully docked **5a** into the ATP-binding pocket of p60, and the theoretically calculated binding affinity is quite high ($\Delta G = -10.7$ kcal/mol). Two plausible binding modes of **5a** in p60 hexamer are shown in Figures 5D and 5E. The predicted binding modes suggested that the backbone nitrogen of Thr256 could bind to the HBA feature of Hypo-1. The interaction to the HBD feature could require the backbone oxygen of Ala358 and the sidechain of Asp308 or Asn360. We also noticed that residues from two subunits of a p60 hexamer contribute to the hydrophobic contacts with **5a**. More specifically, the proposed arginine finger of p60, Arg372, is also involved in the binding to **5a**. Early study demonstrated that ATP induces p60 oligomerization and that the ATP-bound p60 hexamer has a high microtubule severing activity[26]. Based on the docking model presented in this study, we hypothesize that **5a** could stabilize the p60 hexamer structure and enhance the severing activity of katanin. However, this hypothesis requires further experimental investigation.

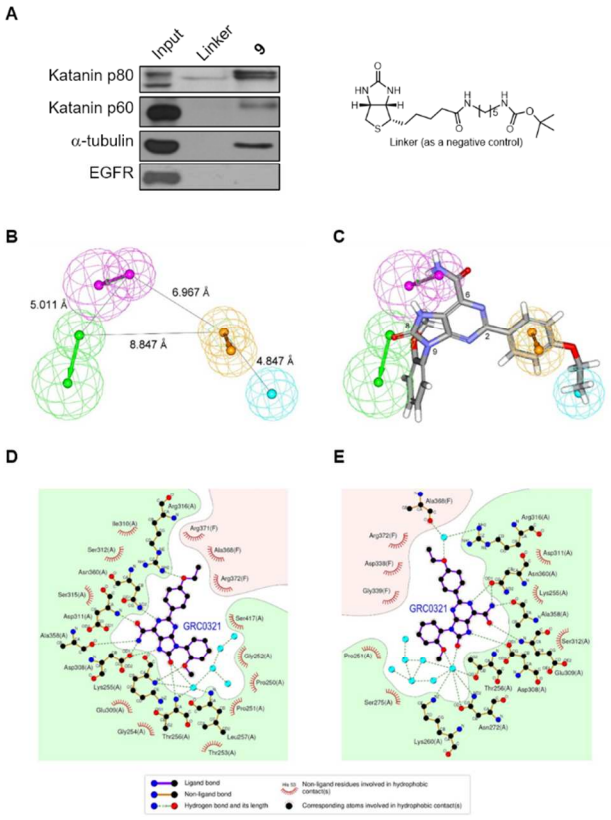

Figure 5. Compound 5a direct interacts with katanin protein as a p60–5a complex. (A) H1975 cell lysate was incubated with probe **9** or a linker without the purine component (as control) for 24 h. Then, the streptavidin-conjugated beads were added into the lysate and incubated for 2 h. The lysate was washed with IP lysis buffer 6 times. The binding proteins were visualized by immunoblotting. The data are representative of three independent experiments. H1975 cells were transfected with scrambled control siRNA or katanin p60 siRNA. (B to E) Pharmacophore model and predicted binding modes between katanin p60 hexamer and **5a**. (B) Best pharmacophore model Hypo-1 represented with distance constraints. (C) Hypo-1 mapping with **5a**. Pharmacophore features are color-coded as follows: green, hydrogen bond acceptor (HBA); magenta, hydrogen bond donor (HBD); cyan, hydrophobic (HY); orange, ring aromatic (RA). (D and E) show two binding modes with equal predicted binding affinities (ΔG = –10.7

kcal/mol). The green background highlights the amino acids from subunit A of the p60 hexamer, and the pink background highlights those that belong to subunit F.

Table 3. Statistical significance, predictive power and features of the top ten hypotheses derived from 3D-QSAR pharmacophore generation.

Hypothesis	Correlation[a]	RMSD[b]	Total cost	ΔCost[c]	Features[d]				Max. Fit
					HBA	HBD	HY	RA	
Hypo-1	0.984	0.699	45.488	54.763	1	1	1	1	8.465
Hypo-2	0.970	0.958	47.619	52.632	1	1	1	1	7.572
Hypo-3	0.958	1.121	49.706	50.545	1	1	2	0	6.849
Hypo-4	0.944	1.290	52.029	48.222	1	1	1	1	6.534
Hypo-5	0.930	1.437	54.039	46.212	1	1	2	0	6.530
Hypo-6	0.916	1.567	55.426	44.825	2	0	1	1	7.272
Hypo-7	0.906	1.657	57.579	42.672	2	1	1	0	6.402
Hypo-8	0.890	1.784	59.697	40.554	2	1	1	0	6.461
Hypo-9	0.822	2.232	68.011	32.240	2	0	1	1	8.615
Hypo-10	0.822	2.228	68.346	31.905	0	0	3	2	8.402

The null cost, fixed cost and configuration cost are 100.251, 42.969 and 18.175, respectively.

[a] Correlation coefficient is calculated based on linear regression derived from the geometric fit index.

[b] Root mean square difference of log(estimated activity) from log(measured activity) normalized to log(uncertainty).

[c] ΔCost= null cost – total cost of the hypothesis.

[d] HBA, hydrogen-bond acceptor; HBD, hydrogen-bond donor; HY, hydrophobic; RA, aromatic ring.

Table 4. Actual and estimated IC_{50} values of 10 purine-type compounds calculated based on the pharmacophore Hypo-1.

Name	Fit[a]	Mapping[b] HBA HBD HY RA	Act.[c] (μM)	Est.[d] (μM)	Error[e]
5e	7.46	[13 11 28 15]	0.19	0.24	+1.3
5a	7.37	[13 11 28 15]	0.30	0.29	-1.0
5c	6.29	[13 11 30 15]	4.66	3.6	-1.3
5f	5.93	[30 * 28 15]	4.73	8.2	+1.7
5b	5.92	[13 11 * 15]	5.80	8.4	+1.4
6e	6.04	[13 11 * 15]	7.91	6.4	-1.2

[a] Fit value is calculated by fitting the chemical features between the hypothesis and the compound; the higher the value is, the better the fit.

[b] Matching degree of the pharmacophore element with the specific conformation of the compound.

[c] Actual IC_{50} value.

[d] Estimated IC_{50} value.

[e] Error factor is calculated as the ratio of the actual IC_{50} to the estimated IC_{50}. A positive value indicates that the estimated IC_{50} is higher than the actual IC_{50}; a negative value indicates that the estimated IC_{50} is lower than the actual IC_{50}.

Compound 5a induces cell apoptosis through interacting with the katanin protein complex. Taking together the results of the probe study and molecular modeling, one can deduce that katanin could be the direct target of **5a**. The microtubule fragmentation phenomenon induced by **5a** was similar to the phenotype observed in the cells that overexpress the katanin protein[27]. To further establish the role of katanin p60 in the anticancer mechanism of **5a**, a katanin p60 knock-down H1975 lung cancer cell line was created by siRNA transfection technology. When treating the katanin p60 silencing cells with **5a**, it would not reduce the amount of α-tubulin in the particulate fraction. The relative expression percentage of the soluble form vs. polymer form was 68% vs. 32% in the siControl group and 34% vs. 66% in the siKatanin group (Figure 6A). Moreover, the microtubule structure was also maintained in a

relatively undamaged status after compound treatment in the siKatanin group compared to the siControl group (Figure 6B). These data all indicated that katanin proteins participated in the mechanism of **5a**-induced microtubule damage in H1975 lung cancer cells.

In addition to the effect of microtubule damage, the apoptotic effects of **5a** could also be reversed by the knock-down katanin p60 protein. First, the phosphorylation levels of JNK and c-Jun were examined by immunoblotting. According to our expectation, the expressions of phospho-JNK and phospho-c-Jun were increased by treatment with **5a** and would reduce significantly in katanin p60 knock-down cells (Figure 6C). Then, the amount of cleaved forms of caspase-3 and PARP-1 induced by treatment with **5a** was also explored in katanin silencing cells. Similar to the findings of phospho-JNK and phospho-c-Jun, increasing amounts of cleaved caspase-3 and PARP-1 after treatment with **5a** were decreased in the knock-down cells (Figure 6D). Finally, the overall cytotoxic effect of **5a** was measured by MTT assay in both the siControl and siKatanin cell groups. The IC_{50} value of this compound increased from 0.25 μM to 0.95 μM (Figure 6E). Taken together, these data indicated that katanin p60 protein is an important protein for regulating **5a**-mediated microtubule damage and apoptosis in H1975 lung cancer cells.

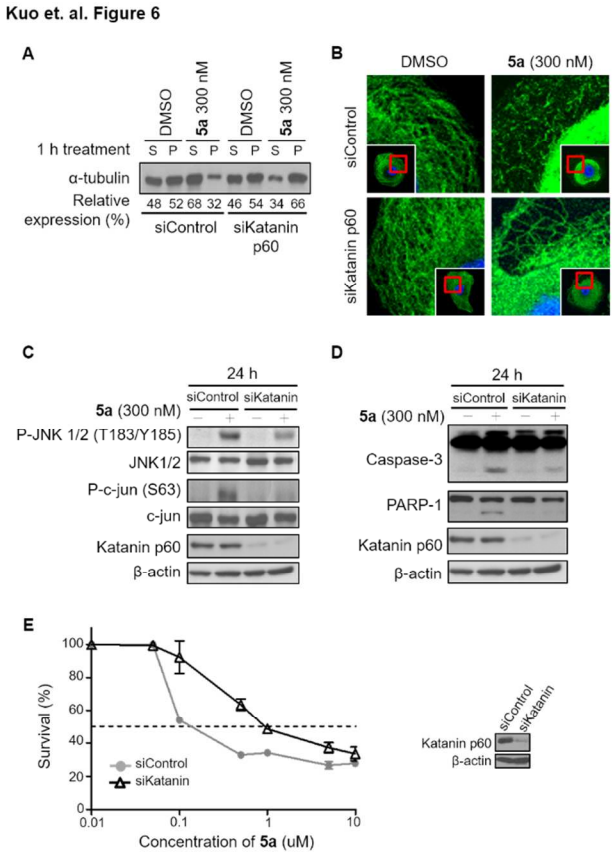

Figure 6. Compound 5a induces cell apoptosis through interacting with the katanin protein complex. (A) The cells were treated with 5a for 1 h. Then, the cells were harvested and separated into soluble (S, tubulin monomer) and particulate (P, tubulin polymers) forms, and the level of α-tubulin protein in each fraction was detected by immunoblotting. The protein level of α-tubulin was quantified using the computerized image analysis system Image J. (B) H1975 cells were incubated with vehicle or 5a for 12 h. Then, the cells were fixed and stained with primary antibody to α-tubulin. FITC-labelled secondary antibodies were used (green fluorescence), and the protein was detected by a confocal laser microscopic system. The nuclei were detected by DAPI staining (blue fluorescence). (C and D) H1975 cells were incubated with vehicle or 5a for 24 h. Then, the cells were harvested for the identification of indicated proteins by immunoblotting. (E) The cell proliferation activity was examined by MTT assay.

DISCUSSION

Microtubules play a crucial role in several cellular processes, especially in the formation of the mitotic spindle during cell mitosis. The disruption of the microtubule dynamics will lead to cell cycle arrest in the G2/M phase; therefore, interference with the microtubule structure has become an important mechanism in anti-cancer therapy. Recently, many MTAs have been developed, and some of them have been approved to enter into clinical trials[28]. In the present study, we demonstrated that the purine-type compound **5a** was a novel MTA that caused microtubule fragmentation by directly targeting the microtubule severing protein, katanin, to induce apoptosis of the cancer cells. Compound **5a** had good *in vitro* and *in vivo* activities against NSCLC, including the gefitinib-resistant types. Compound **5a** also shows a relatively wide therapeutic window between proliferating and quiescent cells (over 10-fold), which indicates that the cell-growth inhibiting effects resulted from inhibiting proliferation-dependent processes rather than indiscriminant cytotoxicity.

By interfering with the microtubule structure, most of the MTAs will cause cancer cell mitotic catastrophe and induce a G2/M cell cycle arrest. The cell cycle arrest allows cells to repair the damage caused by MTAs. However, if the damage cannot be fixed, then the prolonged cell cycle arrest will, in the end, become a stress and trigger a mitochondria-mediated intrinsic apoptosis[10, 29, 30]. Here, we found that **5a**, similar to other MTAs, can induce a sustained G2/M cell cycle arrest and activate intrinsic apoptosis. The release of cytochrome C from mitochondria to the cytosol is a marker for mitochondria-mediated apoptosis, which is controlled by the balance between two subfamilies of Bcl-2 family proteins, the anti-apoptotic and pro-apoptotic subfamilies[31]. Among them, the Bcl-2 protein, as an anti-apoptotic protein, plays an important role in preventing cell apoptosis by binding and neutralizing the activity of pro-apoptotic

subfamily members, such as BAX and BAK. This protecting function of Bcl-2 protein depends not only on their amount in the cytosol but also on their post-transcriptional modification status. Several studies have reported that Cdk1, c-Raf, PKA, JNK1, and p38MAPK kinase can cause the phosphorylation of the Bcl-2 protein; this phosphorylation will then cause a conformational change in the Bcl-2 protein to inactivate the anti-apoptotic function[32, 33]. In our study, after 6-hour of **5a**-treatment, a band with higher molecular weight than unmodified Bcl-2 protein was detected. This band might represent the level of phosphorylated Bcl-2, which implies an inhibitory effect of its function. Because **5a**-treatment would induce a G2/M cell cycle arrest and activation of JNK kinase, we suspected that the phosphorylation of Bcl-2 protein might be caused by the G2/M phase-specific Cdk1 kinase or the JNK kinase.

JNK kinase can phosphorylate different substrates, which include c-Jun, ATF2, ELK1, SMAD4, p53 and HSF1, and it can be involved in different cellular processes, such as apoptosis, neurodegeneration, cell differentiation and proliferation[34]. In the apoptotic pathways, JNK kinase plays opposing roles depending on the upstream stimuli and downstream effectors in the different cells[35]. For example, Ma and his colleagues found that the JNK/c-Jun pathway stimulates cell proliferation and protects cells from apoptosis in a pulmonary artery endothelial cell model[36]. However, in other cell types, such as human lung cancer cells or breast cancer cells, the activation of the JNK/c-Jun pathway will induce caspase-mediated apoptosis[37, 38]. Our studies showed that the JNK/c-Jun pathway could induce cell apoptosis in H1975 human lung cancer cells. The apoptotic effect of **5a** could be alleviated significantly by combining the JNK inhibitor, SP600125. In fact, several studies also reported that different MTAs could activate the JNK/c-Jun pathway to induce an intrinsic apoptosis[39, 40].

Although the effects of **5a** to induce G2/M cell cycle arrest and cell death are similar to those caused by other MTAs, such as taxanes and vinca alkaloids, the target protein and detailed mechanisms of action are different between them. Most of the MTAs directly bind to the tubulin and disrupt the dynamics of microtubule polymerization or depolymerization. The structure of the microtubule will be sustained as a filament when treating the cell with microtubule-stabilizing agents and will disrupt into vague dots when treating with microtubule-destabilizing agents[41, 42]. However, after **5a**-treatment, the microtubules of the cells were cut into fragments instead of dots under microscopic observation. When we further analyzed the dynamics of the microtubules, we found that the rates of microtubule polymerization and depolymerization did not change. To our knowledge, this fragmentation phenotype of microtubule is seldom induced by other MTAs and could imply that a unique microtubule targeting mechanism is used by the purine-type compound **5a**.

Proteins associated with microtubules are responsible for the regulation of microtubule structure[13]. Microtubule severing proteins are one class of proteins that interact with microtubules and regulate microtubule structure by a severing process. Through the severing process, the microtubule will be cut into short fragments and transported to different regions. This arrangement provides an efficient way of promoting microtubule disassembly and movement[16, 43]. Katanin, one of the microtubule severing proteins, has been proven to be an important microtubule structure modulator in many cellular processes[17, 18]. The overexpression of katanin will cause microtubule fragmentation[44, 45]. Because the microtubule structure will undergo intense reorganization in the G2/M phase to help cell division, katanin is also involved in cell dividing processes[46]. McNally and his colleagues proved that katanin p60 will concentrate at the ends of the microtubule and control their lengths in mitotic cells[47]. Maddika and his

colleagues also demonstrated that the overexpression of katanin p60 in HeLa cells causes a G2/M cell cycle arrest and an accumulation of polyploid cells[48]. Our study showed a similar effect of katanin in regulating the microtubule dynamics. Compound **5a** could target both the p60 and p80 subunits of katanin and affect its severing enzyme activity, causing microtubule fragmentation and then cell cycle arrest in the G2/M phase.

The regulation of katanin activity is a complex process that involves chemical modifications, differential degradation and the interactions between katanin and other regulating proteins[18]. One of the major regulating mechanisms works through the cycle of phosphorylation and dephosphorylation of the NDEL1 protein. Cdk proteins, such as Cdk1, can phosphorylate NDEL1 and facilitate NDEL1 association with the p60 subunit of katanin[49, 50]. The NDEL1-associated katanin p60 will tend to concentrate at the centrosome and help break the microtubule into short fragments during cell division[49]. In the present work, because **5a** could cause a G2/M cell cycle arrest, Cdk1, a G2/M-specific kinase, would remain in an activating stage. Therefore, we suspected that the up-regulation of katanin activity after compound treatment could be due to an increase in the phosphorylated NDEL1 by Cdk1 kinase.

CONCLUSION

Currently, taxanes and vinca alkaloids are two of the MTAs that are widely used in clinical treatment. However, the drug resistance poses a major problem after long-term treatment[51]. Most of the mechanisms of resistance to these MTAs are associated with alterations in the microtubule protein itself, including changes in the tubulin isotype expression, posttranslational modifications of tubulin, and the acquisition of tubulin mutations[52, 53]. The purine-type compound (e.g. **5a**), by targeting the microtubule-severing protein katanin, affected the architecture of the microtubules

and caused cancer cell apoptosis. These mechanisms might bypass the major resistant mechanisms that were encountered during most of the MTA treatments. Therefore, **5a** and its analogues could become a novel therapeutic choice for the patients who have MTA-resistant NSCLC.

EXPERIMENTAL SECTION

General. All of the reagents and solvents were reagent grade and were used without further purification unless otherwise specified. All of the solvents were anhydrous grade unless indicated otherwise. CH_2Cl_2 was distilled from CaH_2. All of the non-aqueous reactions were performed in dried glassware and with continuous stirring under an argon or nitrogen atmosphere. The reactions were monitored by thin-layer chromatography on 0.25-mm E. Merck silica gel 60 F_{254} glass plates using $KMnO_4$, *p*-anisaldehyde, ninhydrin and iodine vapor as visualizing agents. E. Merck silica gel 60 (0.040–0.063 mm particle sizes) and LiChroprep RP-18 (0.040–0.063 mm particle sizes) were used for the column chromatography.

Roswell Park Memorial Institute (RPMI) 1640 medium, Dulbecco's Modified Eagle Medium (DMEM) medium and fetal bovine serum (FBS) were obtained from GIBCO/BRL Life Technologies (Grand Island, NY). Antibodies total c-jun, katanin p60, katanin p80, anti-mouse and anti-rabbit IgGs were obtained from Santa Cruz Biotechnology, Inc. (Santa Cruz, CA). Antibodies to poly(ADPribose) polymerase-1 (PARP-1), phosphor-c-jun S63 and caspase-3 were purchased from Cell Signaling Technologies (Boston, MA). Antibodies to β-actin and α-tubulin were obtained from Sigma–Aldrich (St. Louis, MO). Antibodies to phospho-JNK T183/Y185 and total JNK were obtained from Life Technologies. 1-(4,5-Dimethylthiazol-2-yl)-3,5-diphenylformazan (MTT), propidium iodide (PI), phenylmethylsulfonyl fluoride (PMSF),

leupeptin, dithiothreitol (DTT), ethylenediaminetetraacetic acid (EDTA), ethylene glycol tetraacetic acid (EGTA), dimethylsulfoxide (DMSO), Triton X-100, RNase A, sodium orthovanadate, aprotinin, bovine serum albumin (BSA), crystal violet, ammonium persulfate (APS), N,N,N′,N′-tetramethylenediamine (TEMED), sodium dodecylsulfate (SDS), glycine, TRIS hydrochloride and paraformaldehyde were obtained from Sigma-Aldrich. The BCA protein assay kit was obtained from Pierce (Rockford, IL, USA). The fluorescein isothiocyanate (FITC) annexin V apoptosis detection kit was obtained from BD Biosciences (San Jose, CA, USA). The tubulin polymerization assay kit was obtained from Cytoskeleton (Denver, CO, USA). The human phospho-kinase antibody array was obtained from R & D Systems (Minneapolis, MN, USA).

Infrared (IR) spectra were recorded on a Thermo Nicolet iS-5 FT-IR spectrometer. Nuclear magnetic resonance (NMR) spectra were obtained on Bruker Avanced-400 (400 MHz), Bruker AVIII (400 MHz) NMR, Bruker AVIII (500 MHz) NMR or Bruker AVIII (800 MHz) NMR. Chemical shifts (δ) are given in parts per million (ppm) relative to δ_H 7.24/δ_C 77.00 for $CDCl_3$, δ_H 3.31/δ_C 48.15 for CD_3OD, and δ_H 2.49/δ_C 39.50 for DMSO-d_6. The coupling constants (J) are given in hertz (Hz), and the splitting patterns are reported as s (singlet), d (doublet), t (triplet), q (quartet), quint (quintet), m (multiplet) and br (broad). The ESI–HRMS experiments were conducted on a Bruker Daltonics BioTOF III high-resolution mass spectrometer.

New compounds with ≥95% purity were characterized by their physical and spectroscopic properties (mp, IR, ESI−MS, elemental analysis, ^{1}H and ^{13}C NMR).

Identification of 5a by high-throughput screening. A 2-million compound library was used to screen for the anti-proliferation activities against H1975 lung cancer cells at 10μM concentration. The CV% and Z' values of primary screening was determined as 4.9% and 0.58,

respectively. In the screening, about 6800 different small molecules could inhibit more than 80% of H1975 lung cancer cell growth and were selected for the next screening. Eight cell lines, including clinical isolates (CL25, CL83, CL100, CL97, CL141, CL152)[21] as well as 2 ATCC cell lines (PC-9 and PC9/gef, kind gifts from Dr. C. H. Yang, Graduate Institute of Oncology, Cancer Research Center, National Taiwan University) was used in the second screening. The compounds selected from the second screening shall exhibit an IC_{50} value smaller than 6 μM in all texted cell lines. Only 232 small molecules fit the criteria and were selected for the further study. Compound **5a** was one of the hits displaying excellent cytotoxic effects on lung cancer cells and an acceptable therapeutic window between cancer cells and normal cells.

Cell lines and culture conditions. The human lung adenocarcinoma cell line PC9 and derivative PC9/gef clones were gifts from Dr. C. H. Yang (Graduate Institute of Oncology, Cancer Research Center, National Taiwan University). NBE cultured in BEBM (bronchial epithelial basal media) was kindly provided by Dr. Reen Wu (Department of Anatomy, Physiology and Cell Biology, University of California Davis). The human lung adenocarcinoma cell line A549 and H1975 and the normal human foreskin fibroblast cell line HS68 were purchased from American Type Culture Collection (Rockville, MD, USA). The human lung cancer cell lines CL1-0 and CL1-5 were previously selected from an *in vitro* modified Boyden Chamber invasion Assay in our laboratory[54]. In general, PC9, PC9/gef, H1975, CL1-0 and CL1-5 were cultured in RPMI-1640 medium with 10% FBS (v/v) and penicillin (100 units/mL)/ streptomycin (100 μg/mL). A549 and HS68 were cultured in DMEM medium with 10% FBS (v/v) and penicillin (100 units/mL)/ streptomycin (100 μg/mL). Cultures were maintained in a humidified incubator at 37 °C in 5% CO_2/95% air.

MTT assay. Cells were incubated in the absence or presence of the indicated compounds, and the cytotoxic effect was assessed using the MTT assay. The MTT was dissolved in phosphate-buffered saline (PBS) at a concentration of 5 mg/mL and filtered. From the stock solution, 10 μL per 100 μL of medium was added to each well, and the plates were incubated at 37° for 1 h. A yellow tetrazole is reduced to dark blue formazan in living cells, whereas no such reaction would be observed in dead cells. After the loading of MTT, the medium was replaced with 100 μL DMSO for color development, and then, the 96-well plate was read by an enzyme-linked immunosorbent assay (ELISA) reader (540 nm) to obtain the absorbance density values.

Cell cycle analysis. After treatment, the cells were harvested by trypsinization, fixed with 70% (v/v) alcohol at 4 °C for 1 h, and washed with PBS. After centrifugation, the cells were centrifuged and re-suspended with 0.5 mL PI solution that contained RNase (20 μg/mL) and PI (10 μg/mL). The DNA content was analyzed with the FACScan and CellQuest software (Becton Dickinson, Mountain View, CA, USA).

Annexin V and PI staining of apoptosis cells. Cells were cultured in 6-well plates for 24 h and then treated with or without test compound for the indicated amount of time. Then, the cells were washed twice with PBS and stained with FITC annexin V and PI according to the manufacturer's directions. The stained cells were evaluated by the FACScan and CellQuest software.

Immunofluorescence staining. The cells were fixed with 3.7% cold paraformaldehyde and washed with PBS, followed by permeabilization with 0.1% Triton X-100. The cells were then stained with anti-α-tubulin antibody at 37 °C for 1 h; they were washed twice with PBS and incubated with FITC (1:100) conjugated secondary antibody at 37 °C for another 1 h. The cells were mounted onto microscope slides with Prolong® Gold antifade reagent with DAPI

(Molecular Probes) and then examined and photographed using the LSM 700 laser scanning confocal microscope from Carl Zeiss.

Tubulin polymerization assay. After treatment, the cells were harvested by trypsinization and collected by centrifugation. The cells were lysed with 0.1 mL of hypotonic buffer (1 mM $MgCl_2$, 2 mM EGTA, 0.5% NP-40, 2 mM phenylmethylsulphonyl fluoride (PMSF), 200 U/mL aprotinin, 100 μg/mL soy bean trypsin inhibitor, 5.0 mM ε-amino caproic acid, 1 mM benzamidine and 20 mM Tris-HCl, pH 6.8). The cytosolic and cytoskeletal fractions of cell lysate were separated by centrifugation at 16000× g for 15 min. The supernatant contained cytosolic tubulin, and the pellet represented the particulate fraction of polymerized tubulin, which was then re-suspended in 0.1 mL hypotonic buffer. The tubulin content in both fractions was detected by Western blotting.

Gel filtration chromatography. Soluble protein extracts (H1975 cell treated with vehicle or test compound for 12 h) were prepared in IP lysis buffer (20 mM Tris-HCl pH 7.5, 150 mM NaCl, 0.5% Nonidet P-40, 100 μM Na3VO4, 50 mM NaF, 30 mM sodium pyrophosphate plus protease inhibitors). Gel filtration chromatography was performed on a Toyopearl HW-65F resin column (Tosoh Bioscience). The column was equilibrated with 2 column volumes of IP lysis buffer. Each fraction in 0.5 mL (50 mL in total) was separated by 10% SDS–PAGE, and the fractionated proteins were detected with individual antibodies.

Tubulin turbidity assay. Tubulin polymerization and depolymerization were detected by using the tubulin polymerization assay kit (Cytoskeleton Inc.). In both assays, tubulin proteins (> 99% purity) were suspended in general tubulin buffer (G-PEM), buffer containing 80 mM piperazine-N,N'-bis(2-ethanesulfonic acid) (PIPES), 2 mM $MgCl_2$, 0.5 mM EDTA, 1.0 mM GTP (pH 6.9) and 5% glycerol with or without test compound. The mixture was then transferred

to a 96-well plate, and the absorbance was measured at 340 nm at 37 °C (SpectraMAX Plus, Molecular Devices Inc., Sunnyvale, CA, USA).

Phospho-kinase array. Cells were seeded in 100-mm dishes and incubated overnight. Following a 9-h exposure to test compound, the cells were rinsed once with PBS and solubilized with lysis buffer. The lysates were gently rocked at 4 °C for 30 min, and then, they were microcentrifuged for 30 min at 14,000× g. The supernatants were transferred to clean microcentrifuge tubes, and the total protein was quantified by BCA assay. Equivalent amounts of control and treatment lysates were diluted and incubated with the human phospho-kinase proteome profiler array (R&D Systems) according to the manufacturer's protocol. The membranes were then scanned, and the density was measured.

Colony-formation assay. Cells (1×10^3) were seeded in a 6-well dish and incubated at 37 ºC for 24 h. The cells were then incubated in the presence or absence of test compound for 2 weeks. The colonies obtained were washed with PBS and fixed with 3.7% paraformaldehyde, followed by staining with crystal violet.

Immunoblotting. The cells were harvested, washed three times with PBS, and lysed in lysis buffer (0.25 M Tris-HCl, pH 6.8, 0.1% SDS). The protein concentration was measured by BCA assay. Equivalent amounts of cell extracts were loaded into SDS–PAGE and transferred to polyvinylidene membranes (Millipore, Billerica, MA). The membranes were blocked with 5% non-fat milk in PBS buffer that contained 0.1% Tween-20 (Sigma-Aldrich) for 1 h and incubated with respective primary antibody overnight at 4 ºC followed by incubation with appropriate HRP-conjugated secondary antibody for 1 h at room temperature. The signal was visualized by an ECL detection system.

Xenograft tumor growth *in vivo*. BALB/c-nu mice were maintained, and all of the animal procedures were in accordance with the Institutional Animal Care and Use Committee procedures and guidelines. Male BALB/c-nu mice (5 weeks of age) were obtained from National Laboratory Animal Center, Taiwan, and acclimatized to laboratory conditions for 1 week before tumor implantation. Human lung cancer H1975 (3×10^6 cell/mouse) was subcutaneously injected into the flank of the BALB/c-nu mice. Three days after the inoculation of cancer cells, the animals were divided into two groups. Both vehicle and test compound were suspended in DMSO and given intraperitoneally to the animals twice a week for 28 days. The body weight and tumor size were measured each time before drug delivery. The tumor volume was determined by measuring the largest diameters (l) and smallest diameters (s), and the volumes were calculated ($V = 0.5 \times sl^2$).

2-(4-Ethoxyphenyl)-9-(2-methoxyphenyl)-8-oxopurine-6-carboxamide (5a). Compound **3a** was prepared according to the previously reported method.[22] A mixture of diaminomaleonitrile (**1**, 217 mg, 2 mmol) and 2-methoxyphenyl isocyanate (**2a**, 0.28 mL, 2.1 mmol) in anhydrous THF (15 mL) was stirred at room temperature for 24 h under an atmosphere of argon. The mixture was concentrated under reduced pressure. The residual solids were filtered and washed by cold ethanol and diethyl ether to yield the urea **3a** (310 mg, 60% yield).

To a suspension of **3a** (218 mg, 0.85 mmol) and 4-ethoxybenzaldehyde (0.24 mL, 1.74 mmol) in methanol (10 mL), triethylamine (125 μL, 0.89 mmol) was added. The mixture was stirred at room temperature, and the solids dissolved in approximately 1 h. The solution was stirred for another 24 h, during which the solid precipitates gradually formed. The mixture was filtered and washed with cold ethanol and diethyl ether to yield the purine-type **5a** (182.1 mg, 53% yield). $C_{21}H_{19}N_5O_4$; white solid; mp = 261.3–263.2 ^oC; IR ν_{max} (KBr) 3507, 3454, 3290,

3235, 2972, 1744, 1702, 1577 cm^{-1}; ^1H NMR (400 MHz, DMSO-d_6) δ 11.62 (1 H, s, N_7-H), 8.47 (1 H, s, amide), 8.26 (2 H, d, J = 8.8 Hz, H-2″ & H-6″), 7.91 (1 H, s, amide), 7.53 (1 H, dd, J = 8.2, 7.6 Hz, H-4′), 7.46 (1 H, d, J = 7.6 Hz, H-6′), 7.27 (1 H, d, J = 8.2 Hz, H-3′), 7.13 (1 H, dd, J = 8.2, 7.6 Hz, H-5′), 6.93 (2 H, d, J = 8.8 Hz, H-3″ & H-5″), 4.05 (2 H, q, J = 6.8 Hz, OCH_2), 3.73 (3 H, s, OCH_3), 1.32 (3 H, t, J = 6.8 Hz, CH_3); ^{13}C NMR (100 MHz, DMSO-d_6) δ 165.6, 160.2, 160.2, 155.4, 154.8, 153.4, 152.8, 132.7, 130.8, 130.1, 129.2 (2 ×), 129.1, 120.7, 120.6, 114.0 (2 ×), 112.7, 63.1, 55.8, 14.5; ESI–HRMS (negative mode) calculated for $C_{21}H_{18}N_5O_4$: 404.1359, found: *m/z* 404.1374 $[M - H]^-$. Anal. Cacld for ($C_{21}H_{19}N_5O_4$ • ½ H_2O): C, 60.86; H, 4.86; N, 16.90. Found: C, 60.76; H, 5.00; N, 16.74.

2-(4-Hydroxyphenyl)-9-(2-methoxyphenyl)-8-oxopurine-6-carboxamide (5b). By a procedure similar to that for **5a**, the reaction of diaminomaleonitrile urea **3a** (80.6 mg, 0.31 mmol) and 4-hydroxybenzaldehyde (78.4 mg, 0.64 mmol) in the presence of triethylamine (45.8 μL, 0.33 mmol) at room temperature for 24 h gave the purine compound **5b** (38.1 mg, 33% yield). $C_{19}H_{15}N_5O_4$; pale orange solid; mp = 370.2–371.8 °C; IR ν_{max} (KBr) 3472, 3441, 3255, 1732, 1686, 1599, 1510 cm^{-1}; ^1H NMR (400 MHz, DMSO-d_6) δ 11.58 (1 H, br s), 9.77 (1 H, s), 8.40 (1 H, s), 8.17 (2 H, d, J = 7.8 Hz), 7.92 (1 H, s), 7.54 (1 H, dd, J = 8.0, 7.6 Hz), 7.47 (1 H, d, J = 7.6 Hz), 7.28 (1 H, d, J = 8.0 Hz), 7.14 (1 H, dd, J = 8.0, 7.6 Hz), 6.78 (2 H, d, J = 7.8 Hz), 3.73 (3 H, s); ^{13}C NMR (100 MHz, DMSO-d_6) δ 165.7, 159.4, 155.4, 155.3, 153.3, 152.8, 132.8, 130.8, 130.2, 127.9 (2 ×), 120.8, 120.7 (2 ×), 119.1 (2 ×), 112.7 (2 ×), 55.9; ESI–HRMS calculated for $C_{19}H_{16}N_5O_4$: 378.1202, found: *m/z* 378.1201 $[M + H]^+$. Anal. Cacld for ($C_{19}H_{15}N_5O_4$ • ½ CH_3OH): C, 59.54; H, 4.36; N, 17.80. Found: C, 59.50; H, 3.98; N, 18.24.

2-(4-Butoxyphenyl)-9-(2-methoxyphenyl)-8-oxopurine-6-carboxamide (5c). By a procedure similar to that for **5a**, the reaction of diaminomaleonitrile urea **3a** (115 mg, 0.45

mmol) and 4-butoxybenzaldehyde (163.4 mg, 0.92 mmol) in the presence of triethylamine (65.4 μL, 0.47 mmol) at room temperature for 13 h gave the purine compound **5c** (65 mg, 34% yield). $C_{23}H_{23}N_5O_4$; white solid; mp = 268.7–270.2 °C; IR ν_{max} (KBr) 3453, 3277, 3215, 2954, 1744, 1702, 1577 cm^{-1}; ^1H NMR (400 MHz, DMSO-d_6) δ 11.62 (1 H, s), 8.45 (1 H, s), 8.27 (2 H, d, *J* = 8.2 Hz), 7.94 (1 H, s), 7.53 (1 H, dd, *J* = 8.0, 7.6 Hz), 7.47 (1 H, d, *J* = 7.6 Hz), 7.27 (1 H, d, *J* = 8.0 Hz), 7.14 (1 H, t, *J* = 7.6 Hz), 6.94 (2 H, d, *J* = 8.2 Hz), 3.98 (2 H, t, *J* = 6.0 Hz), 3.73 (3 H, s), 1.67 (2 H, m), 1.42 (2 H, m), 0.91 (3 H, t, *J* = 7.2 Hz); ^{13}C NMR (100 MHz, DMSO-d_6) δ 165.7, 160.4, 155.4, 154.9, 153.4, 152.8, 132.8, 130.8, 130.2, 129.24 (2 ×), 129.16, 120.71, 120.68, 114.1 (2 ×), 112.8, 67.2, 55.9, 30.7, 18.7, 13.7; ESI–HRMS calculated for $C_{23}H_{24}N_5O_4$: 434.1828, found: *m/z* 434.1833 $[M + H]^+$. Anal. Cacld for $C_{23}H_{23}N_5O_4$: C, 63.73; H, 5.35; N, 16.16. Found: C, 63.81; H, 5.19; N, 15.85.

2-(4-Hexoxyphenyl)-9-(2-methoxyphenyl)-8-oxopurine-6-carboxamide (5d). By a procedure similar to that for **5a**, the reaction of diaminomaleonitrile urea **3a** (89.3 mg, 0.35 mmol) and 4-hexoxybenzaldehyde (146.8 mg, 0.71 mmol) in the presence of triethylamine (51 μL, 0.37 mmol) at room temperature for 54 h produced the purine compound **5d** (80 mg, 50% yield). $C_{25}H_{27}N_5O_4$; yellow solid; mp = 219.7–220.3 °C; IR ν_{max} (KBr) 3443, 3301, 3129, 2949, 2855, 1760, 1725, 1674 cm^{-1}; ^1H NMR (400 MHz, DMSO-d_6) δ 11.62 (1 H, br s), 8.45 (1 H, s), 8.27 (2 H, d, *J* = 8.8 Hz), 7.94 (1 H, s), 7.54 (1 H, ddd, *J* = 8.0, 7.6, 1.6 Hz, H-4′), 7.47 (1 H, dd, *J* = 7.6, 1.6 Hz, H-6′), 7.27 (1 H, dd, *J* = 8.0, 1.0 Hz, H-3′), 7.14 (1 H, ddd, *J* = 8.0, 7.6, 1.0 Hz, H-5′), 6.93 (2 H, d, *J* = 8.8 Hz), 3.97 (2 H, t, *J* = 6.8 Hz), 3.73 (3 H, s), 1.69 (2 H, quin, *J* = 6.8 Hz), 1.44–1.35 (2 H, m), 1.33–1.25 (4 H, m), 0.86 (3 H, t, *J* = 7.2 Hz); ^{13}C NMR (100 MHz, DMSO-d_6) δ 165.7, 160.4, 155.4, 154.9, 153.4, 152.8, 132.8, 130.8, 130.2, 129.24 (2 ×), 129.18, 120.72, 120.68, 114.1 (2 ×), 112.8, 67.5, 55.9, 31.0, 28.6, 25.2, 22.0, 13.9; ESI–HRMS

calculated for $C_{25}H_{28}N_5O_4$: 462.2141, found: *m/z* 462.2145 $[M + H]^+$. Anal. Cacld for ($C_{25}H_{27}N_5O_4$ • ½ H_2O): C, 63.82; H, 6.00; N, 14.88. Found: C, 64.01; H, 5.83; N, 14.81.

2-(4-Ethoxyphenyl)-9-(3-methoxycarbonyl)phenyl-8-oxopurine-6-carboxamide (5e). The urea compound **3b** was prepared in 78% yield by stirring the mixture of diaminomaleonitrile and 3-(methoxycarbonyl)phenyl isocyanate (**2b**) at room temperature for 15 h. By a procedure similar to that for **5a**, the reaction of urea **3b** (100 mg, 0.35 mmol) and 4-ethoxybenzaldehyde (52 μL, 0.37 mmol) in the presence of triethylamine (52 μL, 0.37 mmol) for 18 h produced the purine compound **5e** (76 mg, 50% yield). $C_{22}H_{19}N_5O_5$; orange solid; mp = 330.5–332.0 °C; IR ν_{max} (KBr) 3456, 3285, 3217, 2983, 2942, 1753, 1701, 1597, 1578 cm^{-1}; ^1H NMR (400 MHz, DMSO-d_6) δ 11.74 (1 H, br s, N_7-H), 8.48 (1 H, s, amide), 8.43 (1 H, t, *J* = 2.0 Hz, H-2′), 8.39–8.36 (2 H, m, H-4′ & H-6′), 8.10–8.01 (2 H, m, H-2″ & H-6″), 7.94 (1 H, s, amide), 7.76 (1 H, dd, *J* = 8.8, 7.4 Hz, H-5′), 6.99–6.96 (2 H, m, H-3″ & H-5″), 4.08 (2 H, q, *J* = 7.2 Hz), 3.91 (3 H, s, CO_2CH_3), 1.34 (3 H, t, *J* = 7.2 Hz); ^{13}C NMR (100 MHz, DMSO-d_6) δ 165.6, 165.6, 160.3, 154.6, 152.6, 133.3, 133.1, 130.5, 130.5, 130.3, 129.4, 129.2 (4 ×), 128.1, 126.5, 114.2 (2 ×), 63.2, 52.4, 14.6; ESI–HRMS calculated for $C_{22}H_{20}N_5O_5$: 434.1464, found: *m/z* 434.1479 $[M + H]^+$. Anal. Cacld for ($C_{22}H_{19}N_5O_5$ • ½ H_2O): C, 59.72; H, 4.56; N, 15.83. Found: C, 59.85; H, 4.55; N, 16.15.

2-(4-Ethoxyphenyl)-9-(4-methoxycarbonyl)phenyl-8-oxopurine-6-carboxamide (5f). The urea compound **3c** was prepared in 90% yield by stirring the mixture of diaminomaleonitrile and 4-(methoxycarbonyl)phenyl isocyanate (**2c**) at room temperature for 20 h. By a procedure similar to that for **5a**, the reaction of urea **3c** (475 mg, 1.67 mmol) and 4-ethoxybenzaldehyde (244 μL, 1.75 mmol) in the presence of triethylamine (244 μL, 1.75 mmol) at 19 h produced the purine compound **5f** (413.6 mg, 58% yield). $C_{22}H_{19}N_5O_5$; orange solid; mp = 264.0–265.3 °C; IR

ν_{max} (KBr) 3439, 3371, 3235, 2983, 1754, 1727, 1685, 1597, 1576 cm^{-1}; ^1H NMR (400 MHz, DMSO-d_6) δ 11.74 (1 H, br s), 8.46 (1 H, s), 8.38 (2 H, br d, J = 8.8 Hz), 8.17 (2 H, br d, J = 8.8 Hz), 7.97 (2 H, br d, J = 8.8 Hz), 7.95 (1 H, s), 6.96 (2 H, br d, J = 8.8 Hz), 4.06 (2 H, q, J = 7.2 Hz), 3.90 (3 H, s), 1.33 (3 H, t, J = 7.2 Hz); ^{13}C NMR (100 MHz, DMSO-d_6) δ 165.7, 165.6, 160.3, 154.8, 152.4, 152.3, 137.1, 133.3, 129.8 (2 ×), 129.3 (2 ×), 129.1, 128.3, 125.7 (2 ×), 119.3, 114.2 (2 ×), 63.2, 52.3, 14.6; ESI–HRMS (negative mode) calculated for $C_{22}H_{18}N_5O_5$: 432.1308, found: *m/z* 432.1218 $[M - H]^-$. Anal. Cacld for ($C_{22}H_{19}N_5O_5 \bullet H_2O$): C, 58.53; H, 4.69; N, 15.51. Found: C, 58.23; H, 4.72; N, 15.87.

2-Biphenyl-9-(3-methoxycarbonylphenyl)-8-oxopurine-6-carboxamide (5g). By a procedure similar to that for **5a**, the reaction of diaminomaleonitrile urea **3b** (30 mg, 0.12 mmol) and 4-phenylbenzaldehyde (44 mg, 0.24 mmol) in the presence of triethylamine (17 μL, 0.13 mmol) for 20 h produced the purine compound **5g** (31 mg, 56% yield). $C_{26}H_{19}N_5O_4$; white solid; mp = 302.3–302.8 ^oC; IR ν_{max} (KBr) 3510, 3455, 3297, 3228, 3064, 3027, 2835, 1728, 1701, 1686, 1594 cm^{-1}; ^1H NMR (400 MHz, DMSO-d_6) δ 11.74 (1 H, s), 8.54 (1 H, s), 8.43 (2 H, d, J = 8.8 Hz), 7.97 (1 H, s), 7.72–7.69 (4 H, m), 7.55 (1 H, dd, J = 8.8, 7.6 Hz), 7.52–7.44 (3 H, m), 7.40–7.35 (1 H, m), 7.30 (1 H, d, J = 8.0 Hz), 7.16 (1 H, td, J = 7.6, 0.8 Hz), 3.75 (3 H, s); ^{13}C NMR (100 MHz, DMSO-d_6) δ 165.6, 155.4, 154.4, 153.4, 141.5, 139.5, 135.9, 132.8, 130.8, 130.2, 129.0 (4 ×), 128.1 (3 ×), 127.8, 126.7 (4 ×), 126.6, 120.7, 112.8, 55.8; ESI–HRMS calculated for $C_{26}H_{19}N_5O_4$: 618.2499, found: *m/z* 618.2486 $[M + H]^+$. Anal. Cacld for ($C_{26}H_{19}N_5O_4 \bullet$ ¼ H_2O): C, 58.53; H, 4.69; N, 15.51. Found: C, 58.23; H, 4.72; N, 15.87.

2-(4-Ethoxyphenyl)-9-(3-carboxy)phenyl-8-oxopurine-6-carboxamide (6e). To a suspension of ester **5e** (100 mg, 0.23 mmol) in pyridine (10 mL), we added 1 M $NaOH_{(aq.)}$ (1 mL). The mixture was stirred at room temperature for 17 h, in which the solids dissolved. The

mixture was stirred for another 5 h until solid precipitates formed. The mixture was concentrated under reduced pressure. The residue was dissolved in methanol and acidified to pH 1.0 by adding 1 M $HCl_{(aq)}$. The suspension was subjected to centrifuge at 8000 rpm for 15 min at 4 °C, and the acid compound **6e** was collected as orange solids (74.8 mg, 78%). $C_{21}H_{17}N_5O_5$; orange solid; mp = 343.7–345.6 °C; IR ν_{max} (KBr) 3446, 2987, 2913, 2509, 1750, 1704, 1600 cm^{-1}; ^1H NMR (400 MHz, DMSO-d_6) δ 11.72 (1 H, s), 8.47 (1 H, s), 8.41–8.34 (3 H, m), 8.02 (2 H, dd, *J* = 8.0, 2.0 Hz), 7.93 (1 H, s), 7.73 (1 H, dd, *J* = 8.0, 7.6 Hz), 6.98–6.95 (2 H, m), 4.07 (2 H, q, *J* = 6.8 Hz), 1.33 (3 H, t, *J* = 6.8 Hz); ^{13}C NMR (100 MHz, DMSO-d_6) δ 166.7, 165.6, 160.3, 154.7, 152.7, 152.6, 133.1, 133.1, 131.6, 130.2, 129.3 (4 ×), 128.4, 126.9, 119.3, 114.2 (2 ×), 63.2, 14.6; ESI–HRMS (negative mode) calculated for $C_{21}H_{16}N_5O_5$: 418.1151, found: *m/z* 418.1159 $[M - H]^-$. Anal. Cacld for ($C_{21}H_{15}N_5Na_2O_5 \bullet CH_3OH$): C, 53.34; H, 3.87; N, 14.14. Found: C, 53.39; H, 4.01; N, 14.21.

2-(4-Ethoxyphenyl)-9-[3-(5-*tert*-butoxycarbonylamino)pentylcarbamoyl]phenyl-8-oxopurine-6-carboxamide (8). To a solution of acid **6e** (72 mg, 0.17 mmol) in anhydrous DMF (5 mL), we added *N,N,N',N'*-tetramethyl-*O*-(1*H*-benzotriazol-1-yl)uronium hexafluorophosphate (HBTU, (78 mg, 0.21 mmol), *N,N*-diisopropylethylamine (36 μL, 0.21 mmol) and 5-(*tert*-butoxycarbonylamino)pentyl amine (**7**, 70 mg, 0.34 mmol). The mixture was stirred at room temperature under argon for 18 h, and then, it was concentrated under reduced pressure. The residue was diluted with CH_2Cl_2 and washed with 1 M $HCl_{(aq)}$, saturated $NaHCO_{3(aq)}$, and brine. The organic phase was dried over $MgSO_4$, filtered, and purified by silica gel chromatography (CH_2Cl_2/MeOH = 19:1), to afford the desired amide product **8** (63 mg, 62%). $C_{31}H_{37}N_7O_6$; yellow solid; mp = 182.2–183.1 °C; TLC (CH_2Cl_2/MeOH= 19:1) R_f = 0.13; IR ν_{max} (KBr) 3356, 2976, 2932, 2865, 1684, 1651, 1597 cm^{-1}; ^1H NMR (400 MHz, DMSO-d_6) δ 11.70 (1 H, s, N_7-

H), 8.52 (1 H, t, *J* = 5.2 Hz, NHBoc), 8.45 (1 H, s, amide), 8.32 (2 H, d, *J* = 8.8 Hz), 8.16 (1 H, s, amide), 7.88–7.84 (2 H, m), 7.83 (1 H, d, *J* = 8.8 Hz), 7.64 (1 H, dd, *J* = 8.0, 7.6 Hz, H-5′), 6.94 (2 H, br d, *J* = 8.8 Hz), 6.71 (1 H, t, *J* = 5.2 Hz, amide), 4.03 (2 H, q, *J* = 6.8 Hz), 3.22 (2 H, t, *J* = 6.0 Hz), 2.84 (2 H, t, *J* = 6.8 Hz), 1.54–1.44 (2 H, m), 1.40–1.21 (16 H, m); ^{13}C NMR (100 MHz, DMSO-d_6) δ 165.6, 165.2, 160.3, 155.6, 154.8, 152.7, 152.7, 135.6, 133.1, 132.8, 129.2 (2 ×), 128.9, 126.3, 125.3, 119.2, 114.1 (2 ×), 77.3, 63.2, 29.2, 29.0, 28.8, 28.2 (3 ×), 23.7, 14.7; ESI–HRMS (negative mode) calculated for $C_{31}H_{36}N_7O_6$: 602.2727, found: *m/z* 602.2714 [M – H]$^-$. Anal. Cacld for ($C_{31}H_{37}N_7O_6$ • 2 H_2O): C, 58.20; H, 6.46; N, 15.33. Found: C, 58.51; H, 6.05; N, 15.22.

Biotin-annexed probe (9). A solution of **8** (63 mg, 0.11 mmol) and TFA (2 mL) in CH_2Cl_2 (2 mL) was stirred at room temperature for 1 h, and then, it was concentrated under reduced pressure to afford the corresponding amine. To a solution of the amine compound in anhydrous DMF (5 mL), HBTU (43 mg, 0.11 mmol), DIEA (27 μL, 0.11 mmol) and a solution of D-(+)-biotin (28 mg, 0.11 mmol) in anhydrous DMF (3 mL) were added. The mixture was stirred at room temperature for 24 h under an atmosphere of argon, and then, it was concentrated under reduced pressure. Methanol (10 mL) was added, and the mixture was centrifuged at 8000 rpm for 15 min at 4 °C. The biotin-annexed compound **9** was collected as yellow solids (48 mg, 73% yield). $C_{36}H_{43}N_9O_6S$; yellow solid; mp = 223.4–224.1 ^{o}C (decomposed); $[\alpha]^{25}_D$ = +272 (DMSO, c = 1); IR ν_{max} (KBr) 3297, 2930, 2860, 1736, 1697, 1598 cm^{-1}; ^{1}H NMR (400 MHz, DMSO-d_6) δ 11.74 (1 H, s), 8.56 (1 H, t, *J* = 5.6 Hz), 8.50 (1 H, s), 8.35 (2 H, d, *J* = 8.8 Hz), 8.21 (1 H, s), 7.94 (1 H, s, H-2′), 7.92 (1 H, d, *J* = 8.0 Hz), 7.87 (1 H, d, *J* = 8.8 Hz), 7.76–7.65 (2 H, m), 6.96 (2 H, d, *J* = 8.8 Hz), 6.40 (1 H, s, biotin-NH), 6.33 (1 H, s, biotin-NH), 4.32–4.25 (1 H, m), 4.13–4.03 (3 H, m), 3.30–3.23 (2 H, m), 3.10–2.98 (3 H, m), 2.82–2.76 (1 H, m), 2.56 (1 H, d, *J*

= 12.4 Hz), 2.02 (2 H, t, *J* = 7.6 Hz), 1.64–1.37 (8 H, m), 1.37–1.20 (7 H, m); ^{13}C NMR (100 MHz, DMSO-d_6) δ 171.8, 165.6, 165.3, 162.7, 160.3, 154.7, 152.7, 135.5, 133.1, 132.9, 129.2 (2 ×), 129.0, 128.8, 126.3, 125.3, 114.1 (2 ×), 63.2, 61.0, 59.2, 55.4, 39.8, 38.3, 35.2, 28.9, 28.8, 28.2, 28.0, 25.3, 23.9, 14.6; ESI–HRMS (negative mode) calculated for $C_{36}H_{44}N_9O_6S$: 730.3135, found: *m/z* 730.3154 $[M + H]^+$. Anal. Cacld for ($C_{36}H_{43}N_9O_6S$ • 2½ H_2O): C, 55.80; H, 6.24; N, 16.27; S, 4.14. Found: C, 56.03; H, 6.07; N, 15.78; S, 4.56.

ASSOCIATED CONTENT

Supporting Information Available:

Additional figures illustrating the body weights and biochemical markers of test mice in anticancer experiments, the procedure of the pharmacophore and organization modeling of **5a** with the katanin p60 subunit, synthetic procedures and compound characterization, and ^{1}H and ^{13}C spectra. This material is available free of charge via the Internet at http://pubs.acs.org.

AUTHOR INFORMATION

Corresponding Author

S.-H. P: phone, 8862-2312-3456 ext. 88661; fax, 8862-3393-6523; E-mail, shpan@ntu.edu.tw.

J.-M. F: phone, 8862-3366-1663; fax, 8862-2363-7812; E-mail, jmfang@ntu.edu.tw.

Notes

The authors declare no competing financial interest.

ACKNOWLEDGMENTS

This work was supported by grants from the National Taiwan University (NTU-CDP-103R7879 and 1104R7879 to S.-H. P) and the Ministry of Science & Technology (105-2911-I-002-303 to P.-C. Y, J.-M. F and NSC 102-2314-B-002-046-MY3 and 103-2923-B-002 -003 to S.-H. P) in Taiwan. We thank the Animal Center of the National Taiwan University College of Medicine for technical service support. We thank supports from Academia Sinica and the research grants from National Research Program for Biopharmaceuticals (ChemBank and High-Throughput Screening Resource Center, NSC-100-2325-B-001-022, NSC-101-2325-B-001-029, and NSC-102-2325-B-001-041).

ABBREVIATIONS USED

AAA, ATPase associated with diverse cellular activities; BUN, blood urea nitrogen; Cre, creatinine; DAPI, 4',6-diamidino-2-phenylindole; DIEA, *N*,*N*-diisopropylethylamine; EGFR, epidermal growth factor receptor; GOT, glutamic oxaloacetic transaminase; GPT, glutamic pyruvic transaminase; HBA, hydrogen-bond acceptor; HBD, hydrogen-bond donor; HBTU, *N*,*N*,*N*',*N*'-tetramethyl-*O*-(1*H*-benzotriazol-1-yl)uronium hexafluorophosphate; HY, hydrophobic feature; JNK, c-Jun N-terminal kinase; MAPs, microtubule-associated proteins; MTA, microtubule targeting agents; MTT, 3-(4,5-dimethylthiazol-2-yl)-2,5-diphenyltetrazolium bromide; NBE, human normal bronchial epithelial cell; NSCLC, non-small-cell lung cancer; PARP-1, poly[ADP-ribose] polymerase 1; PI, propidium iodide; RA, ring aromatic feature; RMSD, lowest root-mean-square deviation; TFA, trifluoroacetic acid; TKIs, tyrosine kinase inhibitors.

Authors will release the atomic coordinates upon article publication.

REFERENCES

1. Siegel, R.; Naishadham, D.; Jemal, A. Cancer statistics, 2012. *Ca-Cancer J. Clin.* **2012**, *62*, 10–29.
2. Nguyen, K. S.; Kobayashi, S.; Costa, D. B. Acquired resistance to epidermal growth factor receptor tyrosine kinase inhibitors in non-small-cell lung cancers dependent on the epidermal growth factor receptor pathway. *Clin. Lung Cancer* **2009**, *10*, 281–289.
3. Nguyen, K. S.; Neal, J. W. First-line treatment of EGFR-mutant non-small-cell lung cancer: the role of erlotinib and other tyrosine kinase inhibitors. *Biologics: Targets & Therapy* **2012**, *6*, 337–345.
4. Camidge, D. R.; Pao, W.; Sequist, L. V. Acquired resistance to TKIs in solid tumours: learning from lung cancer. *Nat. Rev. Clin. Oncol.* **2014**, *11*, 473–481.
5. Higa, G. M. The microtubule as a breast cancer target. *Breast Cancer* **2011**, *18*, 103–119.
6. Stanton, R. A.; Gernert, K. M.; Nettles, J. H.; Aneja R. Drugs that target dynamic microtubules: a new molecular perspective. *Med. Res. Rev.* **2011**, *31*, 443–481.
7. Joshi, M.; Liu, X.; Belani, C. P. Taxanes, past, present, and future impact on non-small cell lung cancer. *Anticancer Drugs* **2014**, *25*, 571–583.
8. Etienne-Manneville, S. From signaling pathways to microtubule dynamics: the key players. *Curr. Opin. Cell Biol.* **2010**, *22*, 104–111.
9. Van der Vaart, B.; Akhmanova, A.; Straube, A. Regulation of microtubule dynamic instability. *Biochem. Soc. Trans.* **2009**, *37*, 1007–1013.
10. Rovini, A.; Savry, A.; Braguer, D.; Carré, M. Microtubule-targeted agents: when mitochondria become essential to chemotherapy. *Biochim. Biophys. Acta* **2011**, *1807*, 679–688.

11. Katsetos, C. D.; Dráber, P. Tubulins as therapeutic targets in cancer: from bench to bedside. *Curr. Pharm. Des.* **2012**, *18*, 2778–2792.

12. Perez, E. A. Microtubule inhibitors: Differentiating tubulin-inhibiting agents based on mechanisms of action, clinical activity, and resistance. *Mol. Cancer Ther.* **2009**, *8*, 2086–2095.

13. Bhat, K. M.; Setaluri, V. Microtubule-associated proteins as targets in cancer chemotherapy. *Clin. Cancer Res.* **2007**, *13*, 2849–2854.

14. Miceli, C.; Tejada, A.; Castaneda, A.; Mistry, S. J. Cell cycle inhibition therapy that targets stathmin in in vitro and in vivo models of breast cancer. *Cancer Gene Ther.* **2013,** 20, 298–307.

15. Rouzier, R.; Rajan, R.; Wagner, P.; Hess, K. R.; Gold, D. L.; Stec, J.; Ayers, M.; Ross, J. S.; Zhang, P.; Buchholz, T. A.; Kuerer, H.; Green, M.; Arun, B.; Hortobagyi, G. N.; Symmans, W. F.; Pusztai, L. Microtubule-associated protein tau: a marker of paclitaxel sensitivity in breast cancer. *Proc. Natl. Acad. Sci. U. S. A.* **2005**, 102, 8315–8320.

16. Sharp, D. J.; Ross, J. L. Microtubule-severing enzymes at the cutting edge. *J. Cell Sci.* **2012**, *125*, 2561–2569.

17. Baas, P. W.; Sharma, V. Cell migration: katanin gives microtubules a trim. *Curr. Biol.* **2011**, *21*, 302–304.

18. Ghosh, D. K.; Dasgupta, D.; Guha, A. Models, regulations, and functions of microtubule severing by katanin. *ISRN Mol. Biol.* **2012**, *2012*, 1–14.

19. Ye, X.; Lee, Y. C.; Choueiri, M.; Chu, K.; Huang, C. F.; Tsai, W. W.; Kobayashi, R.; Logothetis, C. J.; Yu-Lee, L. Y.; Lin, S. H. Aberrant expression of katanin p60 in prostate cancer bone metastasis. *Prostate* **2012**, *72*, 291–300.

20. Sudo, H.; Maru, Y. LAPSER1 is a putative cytokinetic tumor suppressor that shows the same centrosome and midbody subcellular localization pattern as p80 katanin. *FASEB J.* **2007**, *21*, 2086–2100.

21. Yeh, C. T.; Wu, A. T.; Chang, P. M.; Chen, K. Y.; Yang, C. N.; Yang, S. C.; Ho, C. C.; Chen, C. C.; Kuo, Y. L.; Lee, P. Y.; Liu, Y. W.; Yen, C. C.; Hsiao, M.; Lu, P. J.; Lai, J. M.; Wang, L. S.; Wu, C. H.; Chiou, J. F.; Yang, P. C.; Huang, C. Y. Trifluoperazine, an antipsychotic agent, inhibits cancer stem cell growth and overcomes drug resistance of lung cancer. *Am. J. Respir. Crit. Care Med.* **2012**, *186*, 1180–1188

22. Booth, B. L.; Dias, A. M.; Proença, M. F.; Zaki, M. E. A. The reactions of diaminomaleonitrile with isocyanates and either aldehydes or ketones revisited. *J. Org. Chem.* **2001**, *66*, 8436–8441.

23. Davies, J. M.; Brunger, A. T.; Weis, W. I. Improved structures of full-length p97, an AAA ATPase: implications for mechanisms of nucleotide-dependent conformational change. *Structure* **2008**, *16*, 715–726.

24. Kelley, L. A.; Mezulis, S.; Yates, C. M.; Wass, M. N.; Sternberg, M. J. The Phyre2 web portal for protein modeling, prediction and analysis. *Nat. Protoc.* **2015**, *10*, 845–858.

25. Trott, O.; Olson, A. J. AutoDock Vina: improving the speed and accuracy of docking with a new scoring function, efficient optimization, and multithreading. *J. Comput. Chem.* **2010**, *31*, 455–461.

26. Hartman, J. J.; Vale, R. D. Microtubule disassembly by ATP-dependent oligomerization of the AAA enzyme katanin. *Science* **1999**, *286*, 782–785.

27. Yu, W.; Qiang, L.; Solowska, J. M.; Karabay, A.; Korulu, S.; Baas, P. W. The microtubule-severing proteins spastin and katanin participate differently in the formation of axonal branches. *Mol. Biol. Cell* **2008**, *19*, 1485–1498.

28. Liu, Y. M.; Chen, H. L.; Lee, H. Y.; Liou, J. P. Tubulin inhibitors: a patent review. *Expert Opin. Ther. Pat.* **2014**, *24*, 69–88.

29. Gascoigne, K. E.; Taylor, S. S. How do anti-mitotic drugs kill cancer cells? *J. Cell Sci.* **2009**, *122*, 2579–2585.

30. Urra, F. A.; Cordova-Delgado, M.; Pessoa-Mahana, H.; Ramírez-Rodríguez, O.; Weiss-Lopez, B.; Ferreira, J.; Araya-Maturana, R. Mitochondria: a promising target for anticancer alkaloids. *Curr. Top. Med. Chem.* **2013**, *13*, 2171–2183.

31. Czabotar, P. E.; Lessene, G.; Strasser, A.; Adams, J. M. Control of apoptosis by the BCL-2 protein family: implications for physiology and therapy. *Nat. Rev. Mol. Cell Biol.* **2014**, *15*, 49–63.

32. Zhou, L.; Cai, X.; Han, X.; Xu, N.; Chang, D. C. CDK1 switches mitotic arrest to apoptosis by phosphorylating Bcl-2/Bax family proteins during treatment with microtubule interfering agents. *Cell Biol. Int.* **2014**, *38*, 737–746.

33. Wei, Y.; Sinha, S.; Levine, B. Dual role of JNK1-mediated phosphorylation of Bcl-2 in autophagy and apoptosis regulation. *Autophagy* **2008**, *4*, 949–951.

34. Bogoyevitch, M. A.; Kobe, B. Uses for JNK: the many and varied substrates of the c-Jun N-terminal kinases. *Microbiol. Mol. Biol. Rev.* **2006**, *70*, 1061–1095.

35. Chen F. JNK-induced apoptosis, compensatory growth, and cancer stem cells. *Cancer Res.* **2012**, *72*, 379–386.

36. Ma, J.; Zhang, L.; Han, W.; Shen, T.; Ma, C.; Liu, Y.; Nie, X.; Liu, M.; Ran, Y.; Zhu, D. Activation of JNK/c-Jun is required for the proliferation, survival, and angiogenesis induced by EET in pulmonary artery endothelial cells. *J. Lipid Res.* **2012**, *53*, 1093–1105.

37. Avisetti, D. R.; Babu, K. S.; Kalivendi, S. V. Activation of p38/JNK pathway is responsible for embelin induced apoptosis in lung cancer cells: transitional role of reactive oxygen species. *PLoS One* **2014**, *9*, e87050.

38. Deng, Y. T.; Huang, H. C.; Lin, J. K. Rotenone induces apoptosis in MCF-7 human breast cancer cell-mediated ROS through JNK and p38 signaling. *Mol. Carcinog.* **2010**, *49*, 141–151.

39. Kolomeichuk, S. N.; Terrano, D. T.; Lyle, C. S.; Sabapathy, K.; Chambers, T. C. Distinct signaling pathways of microtubule inhibitors--vinblastine and Taxol induce JNK-dependent cell death but through AP-1-dependent and AP-1-independent mechanisms, respectively. *FEBS J.* **2008**, *275*, 1889–1899.

40. Choi, B. H.; Chattopadhaya, S.; Thanh, L. N.; Feng, L.; Nguyen, Q. T.; Lim, C. B.; Harikishore, A.; Nanga, R. P.; Bharatham, N.; Zhao, Y.; Liu, X.; Yoon, H. S. Suprafenacine, an indazole-hydrazide agent, targets cancer cells through microtubule destabilization. *PLoS One* **2014**, *9*, e110955.

41. Jordan, M. A.; Wilson, L. Microtubules as a target for anticancer drugs. *Nat. Rev. Cancer* **2004**, *4*, 253–265.

42. Pasquier, E.; Kavallaris, M. Microtubules: a dynamic target in cancer therapy. *IUBMB Life* **2008**, *60*, 165–170.

43. Roll-Mecak, A.; McNally, F. J. Microtubule-severing enzymes. *Curr. Opin. Cell Biol.* **2010**, *22*, 96–103.

44. Ahmad, F. J.; Yu, W.; McNally, F. J.; Baas, P. W. An essential role for katanin in severing microtubules in the neuron. *J. Cell Biol.* **1999**, *145*, 305–315.

45. Sudo, H.; Baas, P. W. Acetylation of microtubules influences their sensitivity to severing by katanin in neurons and fibroblasts. *J. Neurosci.* **2010**, *30*, 7215–7226.

46. Shiina, N.; Gotoh, Y.; Nishida, E. Microtubule-severing activity in M phase. *Trends Cell Biol.* **1995**, *5*, 283–286.

47. McNally, K.; Audhya, A.; Oegema, K.; McNally, F. J. Katanin controls mitotic and meiotic spindle length. *J. Cell Biol.* **2006**, 175, 881–891.

48. Maddika, S.; Chen, J. Protein kinase DYRK2 is a scaffold that facilitates assembly of an E3 ligase. *Nat. Cell Biol.* **2009**, *11*, 409–419.

49. Toyo-Oka, K.; Sasaki, S.; Yano, Y.; Mori, D.; Kobayashi, T.; Toyoshima, Y. Y.; Tokuoka, S. M.; Ishii, S.; Shimizu, T.; Muramatsu, M.; Hiraiwa, N.; Yoshiki, A.; Wynshaw-Boris, A.; Hirotsune, S. Recruitment of katanin p60 by phosphorylated NDEL1, an LIS1 interacting protein, is essential for mitotic cell division and neuronal migration. *Hum. Mol. Genet.* **2005**, *14*, 3113–3128.

50. Toyo-oka, K.; Mori, D.; Yano, Y.; Shiota, M.; Iwao, H.; Goto, H.; Inagaki, M.; Hiraiwa, N.; Muramatsu, M.; Wynshaw-Boris, A.; Yoshiki, A.; Hirotsune, S. Protein phosphatase 4 catalytic subunit regulates Cdk1 activity and microtubule organization via NDEL1 dephosphorylation. *J. Cell Biol.* **2008**, *180*, 1133–1147.

51. Dumontet, C.; Jordan, M. A. Microtubule-binding agents: a dynamic field of cancer therapeutics. *Nat. Rev. Drug Discovery* **2010**, *9*, 790–803.

52. Kavallaris, M. Microtubules and resistance to tubulin-binding agents. *Nat. Rev. Cancer* **2010**, *10*, 194–204.

53. Huzil, J. T.; Chen, K.; Kurgan, L.; Tuszynski, J. A. The roles of beta-tubulin mutations and isotype expression in acquired drug resistance. *Cancer Inf.* **2007**, *3*, 159–181.

54. Chu, Y. W.; Yang, P. C.; Yang, S. C.; Shyu Y. C.; Hendrix, M. J.; Wu, R.; Wu, C. W. Selection of invasive and metastatic subpopulations from a human lung adenocarcinoma cell line. *Am. J. Respir. Cell Mol. Biol.* **1997**, *17*:353–360

55. Gońka, E.; Chemielewski, P. J.; Lis, T.; Stępień, M. Expanded hexapyrrolohexaazacoronenes. Near-infrared absorbing chromophores with interrupted peripheral conjugation. *J. Am. Chem. Soc.* **2014**, *136*, 16399−16410.

Legends of Figures, Schemes and Tables

Figure 1. Compound 5a inhibits tumor growth in vitro and in vivo. (A) Inhibitory activities of **5a** against different human non-small-cell lung cancer cell lines. The cells were treated with **5a** for 72 h, and cell proliferation was examined by MTT assay. Data are expressed as the mean of four determinations. (B) H1975 cells were treated with **5a** (300 nM) for 14 days. The colonies were fixed and stained with crystal violet and counted. Data are expressed as the mean ±SEM of three determinations. (C) H1975 cells were injected subcutaneously into the right flank region of nude mice. Three days after the injection, the mice were treated with vehicle (DMSO) or **5a** (2 mg/kg) twice a week intraperitoneally for 28 days. Representative tumor images and H&E-stained sections of tumors taken from mice treated for 28 days with either vehicle or **5a** are shown. The tumor size was measured with a caliper rule every time before compound delivery. Data are presented as the mean tumor volumes of mice in both the treatment and vehicle groups on the days of pre-treatment.

Figure 2. Compound 5a causes cell cycle arrest and induces cell apoptosis in H1975 lung cancer cells. H1975 cells were treated with 300-nM **5a** for the indicated time periods. Then, the cells were harvested for (A) annexin V-PI double staining of apoptosis FACScan flow cytometer. Data are expressed as the mean ±SEM of three determinations. (B and C) The protein expressions were detected by immunoblotting. The data are representative of three independent experiments. (D) The cytosolic and mitochondrial fractions were obtained for the detection of the cytochrome C protein level by immunoblotting. (E) The cells were fixed and stained with PI to analyze the DNA content with a FACScan flow cytometer. The data are representative of three independent experiments.

Figure 3. JNK-related signaling pathway involved in 5a-induced cancer cell apoptosis. (A) H1975 cells were incubated in the absence or presence of **5a** (300 nM) for 9 h. The cells were then harvested and lysed to detect the phosphorylation level of the proteins included in the human phosphor-kinase antibody array. The phosphorylation level of particulate proteins was quantified using the computerized image analysis system ImageJ. (B) H1975 cells treated with **5a** (300 nM) were harvested and lysed to detect the existence of phospho-JNK and phospho-c-Jun. The data are representative of three independent experiments. (C) H1975 cells were incubated in the indicated agent (**5a**, 300 nM; SP600125, 10 μM) for 48 h. Then, the cells were harvested and lysed to examine the expression levels of cleavage caspase-3, PARP-1 and phospho-c-Jun. The data are representative of three independent experiments. (D) H1975 cells were treated with the indicated agent (**5a**, 300 nM; SP600125, 10 μM) for 48 h. Then, the cells were harvested for the annexin V-PI double staining of the apoptosis FACScan flow cytometer. The data are expressed as the mean ±SEM of three determinations.

Figure 4. Treatment of 5a interrupts microtubule organization in H1975 lung cancer cells. (A) H1975 cells were incubated with vehicle or **5a** (300 nM) for the indicated times. Then, the cells were fixed and stained with anti-α-tubulin primary antibody. FITC-labelled secondary antibodies were used (green fluorescence), and the protein was detected by a confocal laser microscopic system. The nuclei were detected by DAPI staining (blue fluorescence). (B) H1975 cells were incubated with vehicle, **5a**, paclitaxel or nocodazole for 1 h. Then, the cells were harvested and separated into soluble (S, tubulin monomer) and particulate form (P, tubulin polymers), and the level of α-tubulin protein in each fraction was detected by immunoblotting. The protein level of α-tubulin was quantified using the computerized image analysis system ImageJ. (C) H1975 cells were incubated in the absence

or presence of **5a** (300 nM) for 12 h. Then, the cells were harvested and lysed for gel filtration chromatography. The drop-by-drop flowthrough was collected in ~0.5-mL fractions. The protein level of α-tubulin in each fraction was detected by immunoblotting. (D) Purified tubulins were incubated at 37 ^{o}C with GTP in the vehicle (control) or in the presence of **5a** (10 μM or 300 nM), paclitaxel (10 μM), vincristine (10 μM) or nocodazole (10 μM). Tubulin polymerization was examined turbidimetrically. Data are expressed as the mean of three determinations. (E) Purified tubulins were incubated with GTP and paclitaxel at 37 ^{o}C for 30 min and then were held at room temperature for at least 1 h to obtain microtubule stock. The microtubule stock was further incubated at 37 ^{o}C with GTP in the vehicle (control) or in the presence of **5a** (10 μM, 3 μM or 300 nM), paclitaxel (30 μM) or vincristine (30 μM). Tubulin depolymerization was examined turbidimetrically. The data are expressed as the mean of three determinations.

Figure 5. Compound 5a direct interacts with katanin protein as a p60–5a complex. (A) H1975 cell lysate was incubated with probe **9** or a linker without the purine component (as control) for 24 h. Then, the streptavidin-conjugated beads were added into the lysate and incubated for 2 h. The lysate was washed with IP lysis buffer 6 times. The binding proteins were visualized by immunoblotting. The data are representative of three independent experiments. H1975 cells were transfected with scrambled control siRNA or katanin p60 siRNA. (B to E) Pharmacophore model and predicted binding modes between katanin p60 hexamer and **5a**. (B) Best pharmacophore model Hypo-1 represented with distance constraints. (C) Hypo-1 mapping with **5a**. Pharmacophore features are color-coded as follows: green, hydrogen bond acceptor (HBA); magenta, hydrogen bond donor (HBD); cyan, hydrophobic (HY); orange, ring aromatic (RA). (D and E) show two binding modes with equal predicted

binding affinities (ΔG = –10.7 kcal/mol). The green background highlights the amino acids from subunit A of the p60 hexamer, and the pink background highlights those that belong to subunit F.

Figure 6. Compound 5a induces cell apoptosis through interacting with the katanin protein complex. (A) The cells were treated with 5a for 1 h. Then, the cells were harvested and separated into soluble (S, tubulin monomer) and particulate (P, tubulin polymers) forms, and the level of α-tubulin protein in each fraction was detected by immunoblotting. The protein level of α-tubulin was quantified using the computerized image analysis system Image J. (B) H1975 cells were incubated with vehicle or 5a for 12 h. Then, the cells were fixed and stained with primary antibody to α-tubulin. FITC-labelled secondary antibodies were used (green fluorescence), and the protein was detected by a confocal laser microscopic system. The nuclei were detected by DAPI staining (blue fluorescence). (C and D) H1975 cells were incubated with vehicle or 5a for 24 h. Then, the cells were harvested for the identification of indicated proteins by immunoblotting. (E) The cell proliferation activity was examined by MTT assay.

Scheme 1. Synthesis of purine-type compounds **5a**–**5g**.

Scheme 2. Synthesis of amides **8** and the biotin-annexed probes **9**.

Table 1. Inhibitory activities of **5a** against different lung cell lines.

Table 2. Inhibitory activities of purine-type compounds against the growth of H1975 lung cancer cells.

Table 3. Statistical significance, predictive power and features of the top ten hypotheses derived from 3D-QSAR pharmacophore generation.

Table 4. Actual and estimated IC_{50} values of the 10 purine-type compounds calculated based on the pharmacophore Hypo-1.

Table of Content (Graphics)

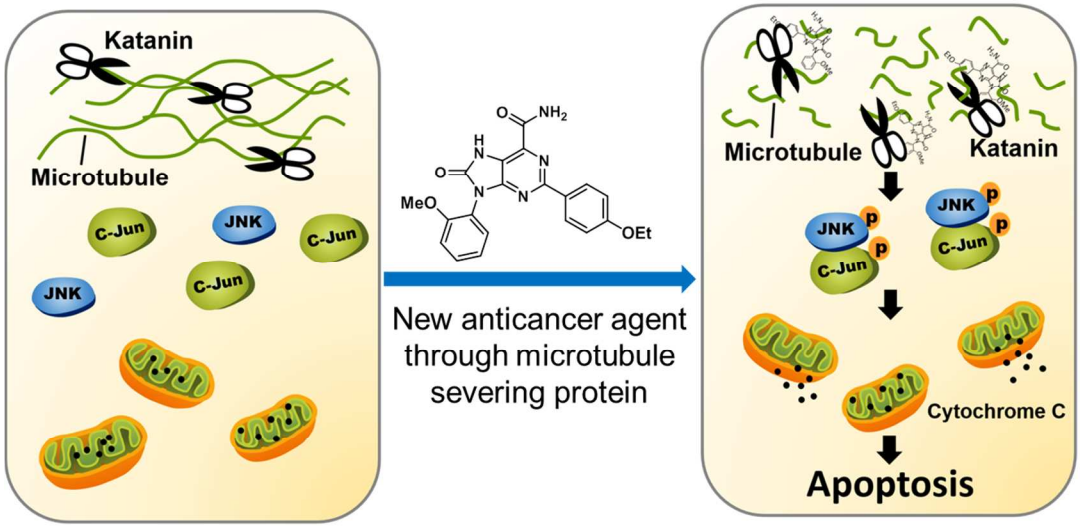

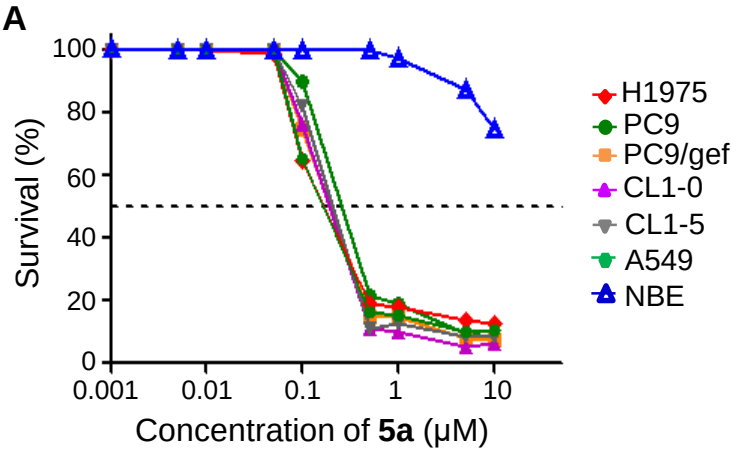
A
Survival (%)
100
80
60
40
20
0
0.001
0.01
0.1
1
10
Concentration of 5a (μM)
H1975
PC9
PC9/gef
CL1-0
CL1-5
A549
NBE

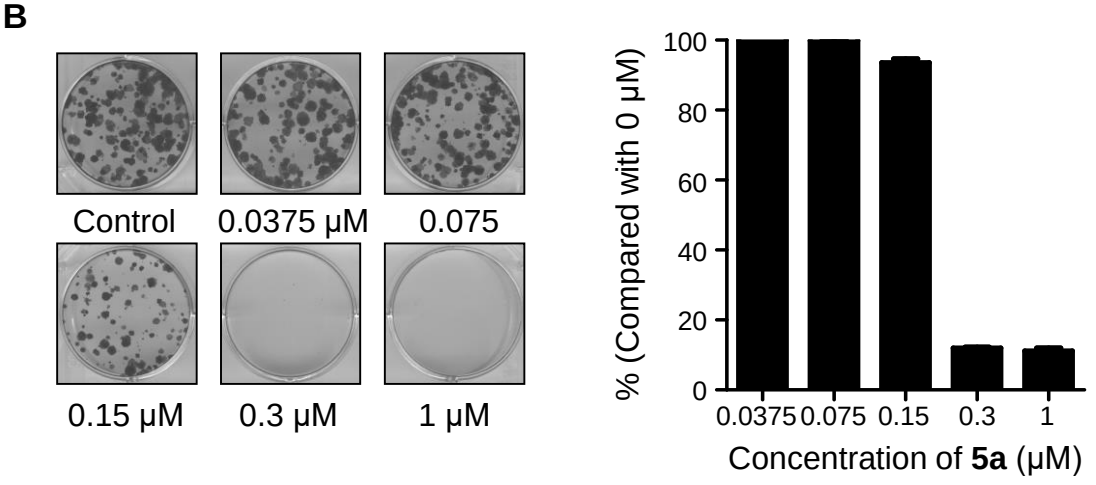
B
Control
0.0375 μM
0.075
0.15 μM
0.3 μM
1 μM
% (Compared with 0 μM)
100
80
60
40
20
0
0.0375
0.075
0.15
0.3
1
Concentration of 5a (μM)

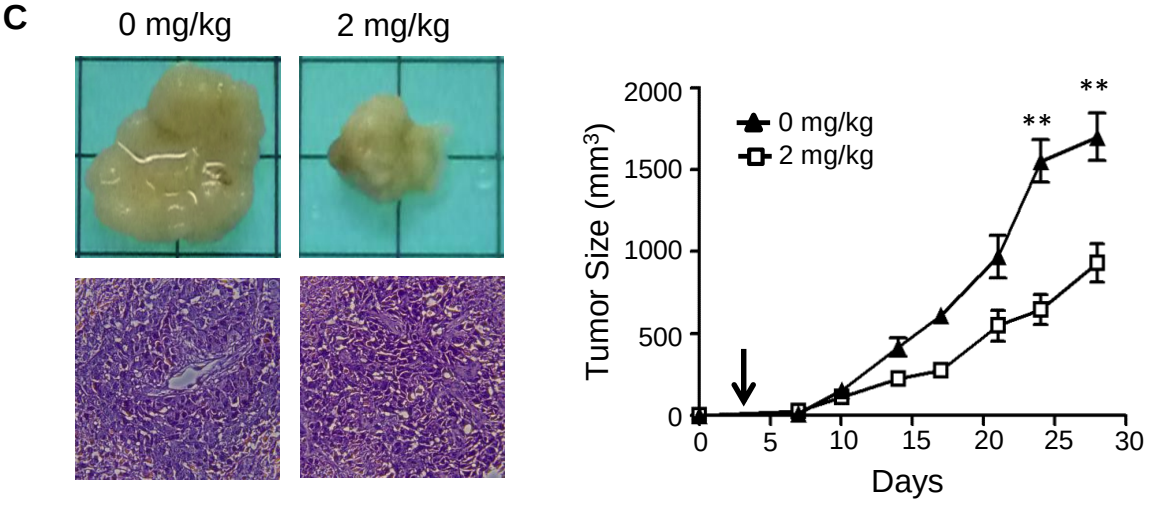
C
0 mg/kg
2 mg/kg
Tumor Size (mm3)
2000
1500
1000
500
0
0
5
10
15
20
25
30
Days
0 mg/kg
2 mg/kg
**
**

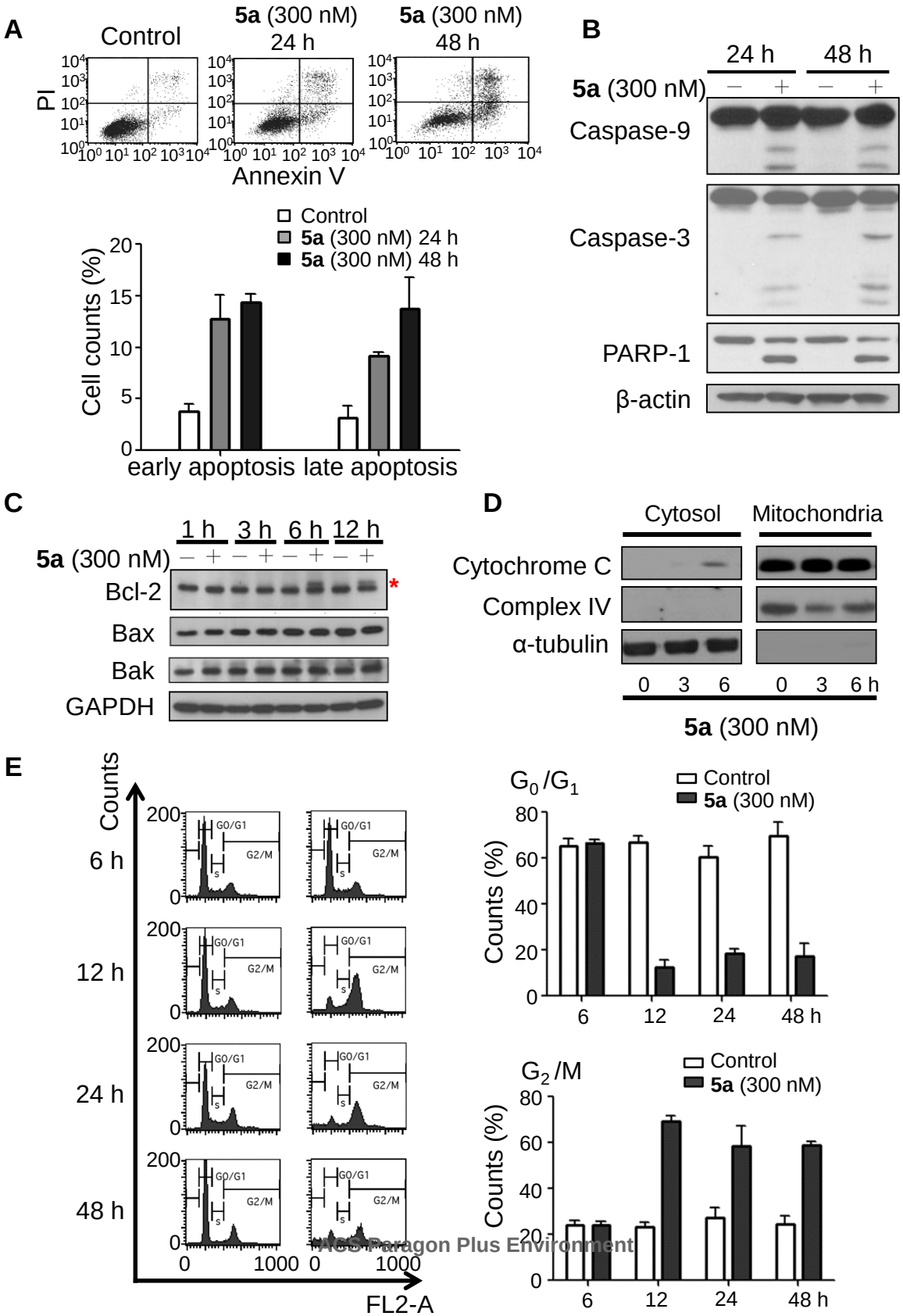

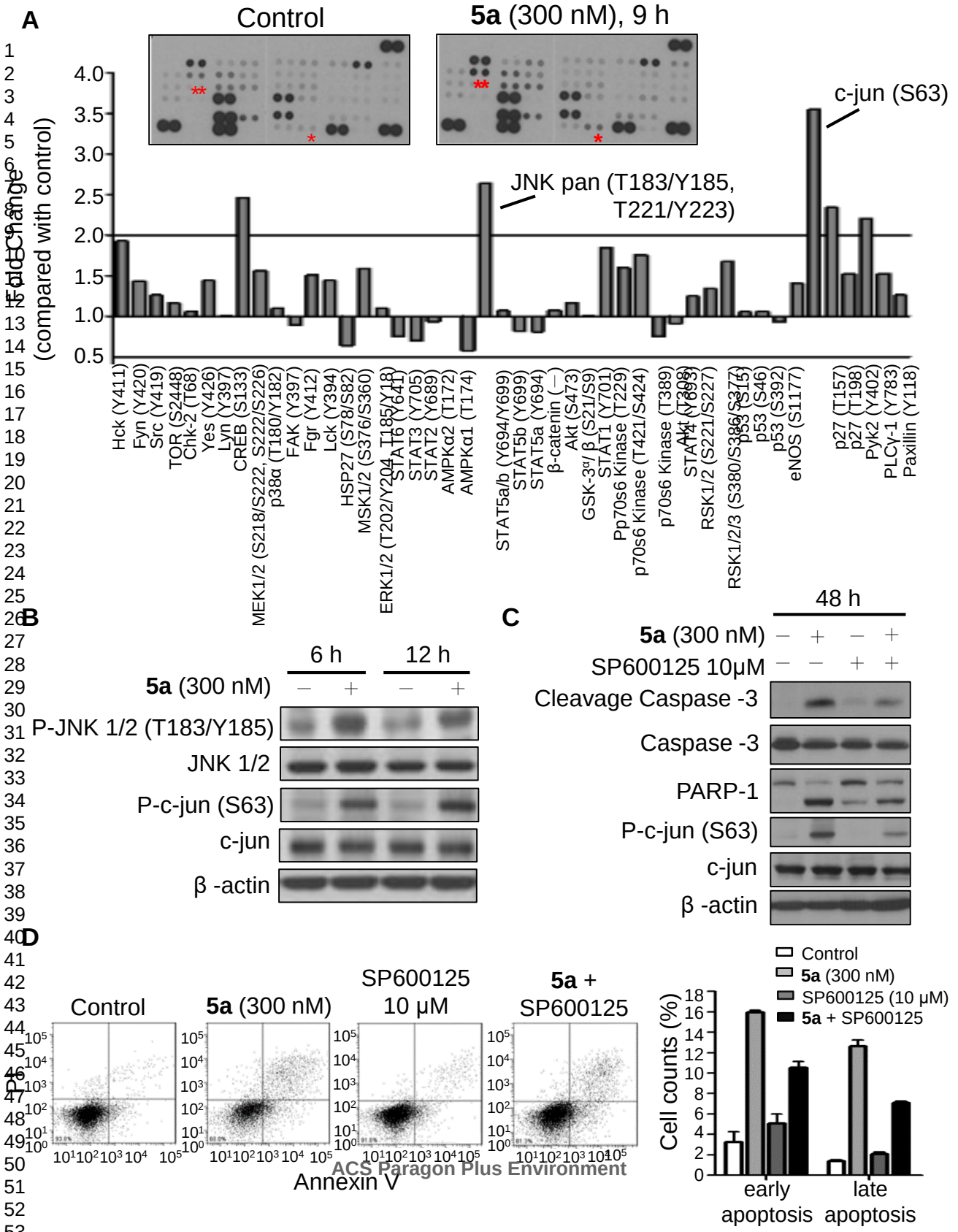

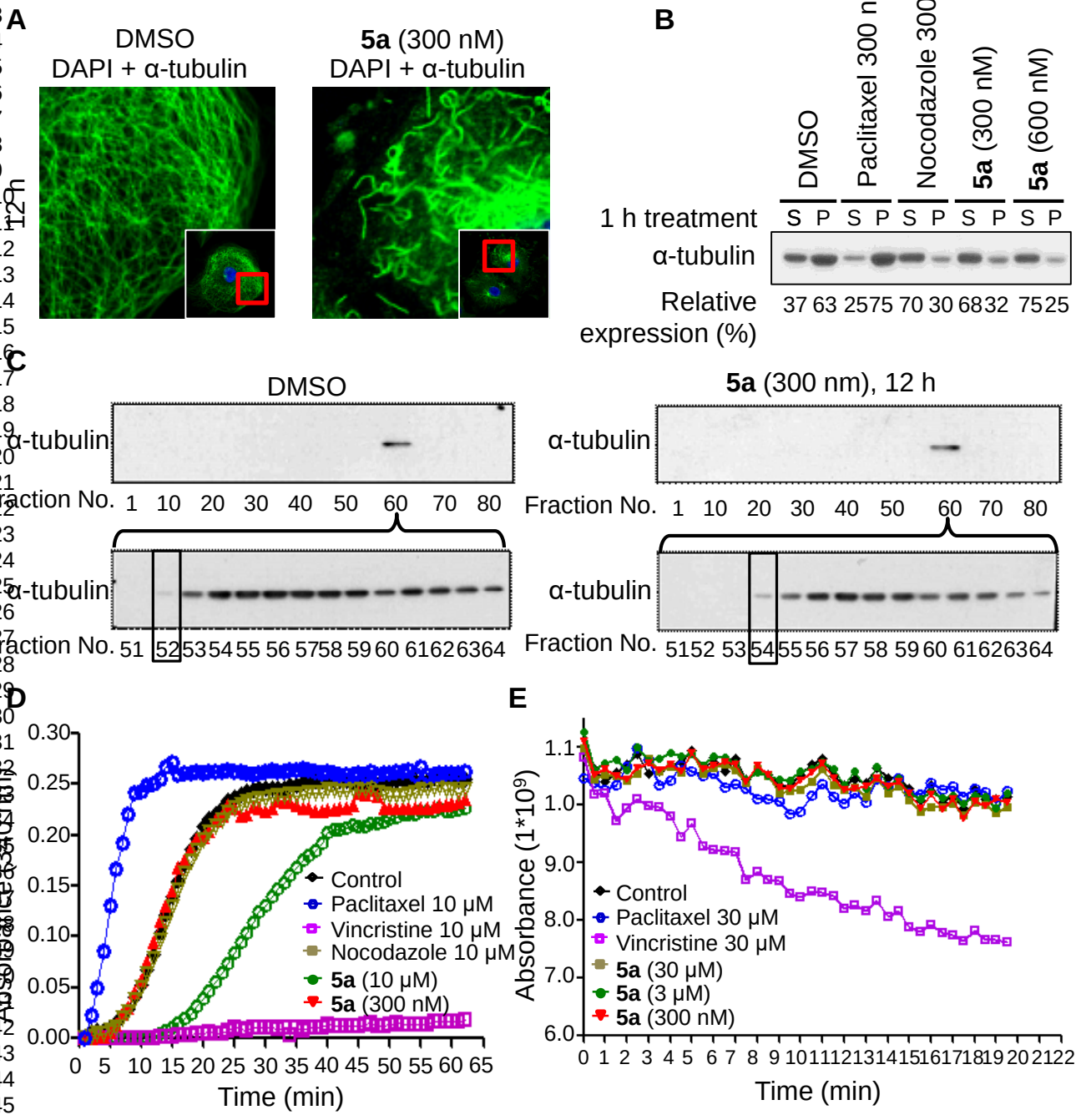
A
DMSO
DAPI + α-tubulin
5a (300 nM)
DAPI + α-tubulin
12 h
B
DMSO
Paclitaxel 300 nM
Nocodazole 300 nM
5a (300 nM)
5a (600 nM)
1 h treatment
S P S P S P S P S P
α-tubulin
Relative expression (%)
37 63 25 75 70 30 68 32 75 25
C
DMSO
5a (300 nm), 12 h
α-tubulin
Fraction No. 1 10 20 30 40 50 60 70 80
α-tubulin
Fraction No. 51 52 53 54 55 56 57 58 59 60 61 62 63 64
α-tubulin
Fraction No. 1 10 20 30 40 50 60 70 80
α-tubulin
Fraction No. 51 52 53 54 55 56 57 58 59 60 61 62 63 64
D
Absorbance (570 nm)
0.30
0.25
0.20
0.15
0.10
0.05
0.00
0 5 10 15 20 25 30 35 40 45 50 55 60 65
Time (min)
Control
Paclitaxel 10 μM
Vincristine 10 μM
Nocodazole 10 μM
5a (10 μM)
5a (300 nM)
E
Absorbance (1*10^9)
1.1
1.0
9.0
8.0
7.0
6.0
0 1 2 3 4 5 6 7 8 9 10 11 12 13 14 15 16 17 18 19 20 21 22
Time (min)
Control
Paclitaxel 30 μM
Vincristine 30 μM
5a (30 μM)
5a (3 μM)
5a (300 nM)